NOVA SCHOOL OF SCIENCE & TECHNOLOGY

DEPARTAMENT OF MATERIAL SCIENCES

RUI PEDRO MARTINS FELIZARDO

BSc in Micro and Nanotechnologies Engineering

Aluminum doping of zinc oxide thin films produced by atomic layer deposition for transparent conductors

MSc IN MICRO AND NANOTECHNOLOGIES ENGINEERING

NOVA University of Lisbon

December, 2021

NOVA

NOVA SCHOOL OF
SCIENCE & TECHNOLOGY

DEPARTAMENT OF MATERIALS SCIENCES

Aluminum doping of zinc oxide thin films produced by atomic layer deposition for transparent conductors

RUI PEDRO MARTINS FELIZARDO

BSc in Micro and Nanotechnology Engineering

Adviser: Pedro Miguel Cândido Barquinha, Ph.D.,
Associate Professor, NOVA University Lisbon

Co-advisers: Jonas Deuermeier, Ph.D.,
Assistant Professor, NOVA University Lisbon

Examination Committee:

Chair: Rodrigo Ferrão de Paiva Martins, Ph.D.,
Full Professor, NOVA University of Lisbon

Rapporteurs: Ian Povey, Ph.D.,
Researcher, Tyndall Institute

Members: Jonas Deuermeier, Ph.D.,
Assistant Professor, NOVA University of Lisbon

MSc IN MICRO AND NANOTECHNOLOGIES ENGINEERING

NOVA University Lisbon
December, 2021

Production of AZO thin films by ALD for TCO applications

Copyright © Rui Felizardo, NOVA School of Science and Technology, NOVA University Lisbon.
The NOVA School of Science and Technology and the NOVA University Lisbon have the right, perpetual and without geographical boundaries, to file and publish this dissertation through printed copies reproduced on paper or on digital form, or by any other means known or that may be invented, and to disseminate through scientific repositories and admit its copying and distribution for non-commercial, educational or research purposes, as long as credit is given to the author and editor.

Para a minha mãe,

ACKNOWLEDGMENTS

Serve este primeiro parágrafo para reconhecer todo o trabalho e dedicação por parte do prof. Dr. Rodrigo Martins e prof. Dra. Elvira Fortunato, não só pela criação das instalações CENIMAT|I3N e CEMOP, onde pude realizar a minha tese de mestrado, mas também pela conceção do curso de Engenharia de Micro e Nanotecnologias, curso este que se revelou como uma incrível experiência.

Quero também agradecer a todos os professores da FCT-UNL que tiveram um direto impacto na minha vida académica, em particular ao corpo docente do Departamento de Ciência dos Materiais que moldou o meu percurso ao longo destes cinco anos. Assim sendo, vejo-me compelido a dar um agradecimento especial aos meus orientadores, o Prof. Dr. Pedro Barquinha e o Prof. Dr. Jonas Deuermeier que ao longo da minha tese me ofereceram conhecimento incrivelmente valioso e cujas palavras de apoio, motivação e reconhecimento me ajudaram imenso. Digo, na maior das sinceridades, que nunca esquecerei a vossa ajuda e dedicação. Claro que não me posso esquecer de toda a equipa da câmara limpa que me acompanhou e ajudou nestes últimos meses! Quero agradecer em particular à Ana Santa, cuja incrível paciência, apoio na aprendizagem das diferentes técnicas/metodologias necessárias para realizar este trabalho e total assistência sempre que necessário, me fizeram concluir que faz mais do que jus ao apelido, e à Mariana Cortinhal, cuja experiência no ALD e total disponibilidade para me ajudar, me fez aprender muito mais do que alguma vez poderia pedir (e claro, também tenho de dizer que as súbitas conversas sobre o porquê de viagens no tempo e teletransporte não funcionarem no mundo real eram sempre interessantes). Muito obrigado pelo vosso apoio!

Agora, não posso só agradecer ao pessoal com quem estive a fazer a tese, portanto quero dedicar este parágrafo a todos os meus amigos, dentro e fora da faculdade, que me acompanharam e apoiaram ao longo deste tempo. Dou assim um agradecimento especial ao Dani, Freire e Inácio por todas as gargalhadas originadas através de humor extremamente duvidoso e sessões de *gaming* em que acabávamos sempre por, carinhosamente, mandar vir uns com os outros (especialmente tu Dani, mas não podemos ser bons em tudo), à Madalena, por toda a companhia e apoio em trabalhos nos quais queimámos imensas pestanas e pelas conversas e teorias sobre o que iria acontecer no próximo filme/série da Marvel e à Liliya que, apesar de ter ido para terras longínquas, foi uma das melhores pessoas que podia ter conhecido. No que toca a amigos fora da faculdade (empreendedorismo não conta) quero agradecer à Ana, Bara e Bruno que, apesar de nem sempre concordarmos, especialmente quando eu digo (e bem) que uma dada série é overrated, sempre estiveram lá para mim, tanto nos bons e nos maus momentos, e cujas chamadas de Discord onde falávamos até tarde desde as coisas mais banais às histórias mais pessoais me fizeram, na minha genuína opinião, crescer enquanto pessoa. Digo-vos assim que mal posso esperar por finalmente concretizarmos o nome deste nosso grupo e irmos todos ao Japão!

Por fim, quero reservar o maior agradecimento à minha família, em particular à minha irmã e à minha mãe. Começando por ti "oh maninha", muito obrigado por todos estes anos espetaculares. Apesar de muitas vezes andarmos às turras (como todos os irmãos fazem…) e que chateiam sempre a nossa mãe, adoro-te e desejo-te todo o sucesso do mundo. Muito obrigado, mãe, por estes incríveis 22 anos, desde os momentos em que era uma criança e te chateava com a pergunta "Mãe, gostas de mim?", pergunta à qual respondias sempre que sim, com um terno sorriso, até aos dias de hoje, em que posso dizer que as minhas maiores qualidades se devem a todo o esforço e dedicação da mulher mais forte que conheço. Muito obrigado por tudo!

“Never let the future disturb you. You will meet it, if you have to, with the same weapons of reason which today arm you against the present." (Marcus Aurelius).

ABSTRACT

Transparent conducting oxides (TCOs) serve as a technological necessity in a multitude of industries, being used in a vast array of devices, from photovoltaic cells to transparent electronics. However, high economical costs and growing environmental concerns have led to the decline in popularity of many key materials that are able to produce TCOs. This has, understandably, led to the research and development of new materials and technologies that are able to be produce TCOs in a cost-effective/environmentally-friendly fashion, while still retaining the desired electrical properties.

In the present work, atomic layer deposition (ALD) was employed in order to produce conformal and uniform zinc oxide (ZnO) and aluminum-doped zinc oxide (AZO) thin films. The deposition process of ZnO was optimized within a range of temperatures between 100-200 ºC, with a typical ALD regime being achieved within the interval 125-150 ºC, after the tuning of precursor pulses times.

After the aforementioned optimization, AZO films were produced at a temperature of 150 ºC, of which the morphological and electrical properties were investigated as a function of dopant concentration. Promising results were achieved, with an aluminum concentration of 1.98% attaining bulk resistivity and Hall mobility of 6.65×10^{-3} Ω*cm and 7.06 cm^2/V*s, respectively. This opens the possibility to produce conformal and uniform films capable of attaining good electrical properties while employing a smaller thermal budget, facilitating film depositions on top of more temperature sensitive substrates.

Keywords: TCO, ALD, ZnO, AZO, bulk resistivity, Hall mobility, carrier concentration, low temperature

RESUMO

Óxidos condutores transparentes (TCOs) são uma necessidade tecnológica numa variedade de indústrias, sendo utilizados numa vasta gama de dispositivos, desde células fotovoltaicas à eletrónica transparente. Contudo, elevados custos financeiros e crescentes preocupações ambientais levaram à diminuição da popularidade de materiais capazes de produzir TCOs. Isto levou, compreensivelmente, ao estudo e desenvolvimento de novos materiais e tecnologias capazes de desenvolver TCOs de formas financeiramente eficazes e ambientalmente conscientes, mantendo mesmo assim as propriedades elétricas desejadas.

No presente trabalho, atomic layer deposition (ALD) foi empregue para produzir filmes finos uniformes e conformais de óxido de zinco (ZnO) e óxido de zinco dopado com alumínio (AZO). O processo de deposição do ZnO foi otimizado num intervalo de temperaturas entre 100-200 ºC, tendo-se obtido um típico regime de ALD entre 125-150 ºC, após o ajuste dos tempos de pulso do precursor.

Após a supramencionada otimização, filmes de AZO foram fabricados usando uma temperatura de 150 ºC, analisando-se as propriedades morfológicas e elétricas em função da concentração de dopante. Foram obtidos resultados promissores, sendo que com uma concentração de alumínio de 1.98% se obteve uma resistividade e mobilidade de Hall de 6.65×10^{-3} Ω*cm e 7.06 cm^2/V*s, respetivamente. Assim, existe a possibilidade de criar filmes conformes e uniformes capazes de obter boas propriedades elétricas usando processos de baixa temperatura, permitindo a deposição de filmes em substratos mais sensíveis à temperatura.

Palavas chave: TCO, ALD, ZnO, AZO, resistividade, mobilidade de Hall, concentração de portadores, baixa-temperatura

CONTENTS

1 INTRODUCTION 3
1.1 Transparent conducting oxides (TCOs) 3
1.1.1 AZO: A suitable substitute 3
1.2 Atomic Layer Deposition 4
1.2.1 ALD of ZnO/AZO 5
1.2.2 AZO: A literary overview 6
2 MATERIALS AND METHODS 9
2.1 Thin film deposition 9
2.2 Thin film characterization 10
3 RESULTS AND DISCUSSION 11
3.1 Film growth and morphology 11
3.1.1 Ellipsometry 11
3.1.2 FTIR 12
3.1.3 SEM/EDS 14
3.1.4 XRD/GIXRD 16
3.2 Electrical properties 17
3.2.1 Hall measurements 17
3.3 XPS 20
3.3.1 Analysis of the ZnO/Al_2O_3 interface 20
3.3.2 Overlayer thickness measurements 22
4 CONCLUSIONS AND FUTURE PERSPECTIVES 25
5 REFERENCES 27
6 ANNEXES 29

LIST OF FIGURES

Figure 1.1 — Illustration of a typical ALD cycle. In this process, a metallic precursor is introduced into the chamber, depicted through Pulse A. After all surface functional groups have reacted with this precursor, a purge step removes all unreacted precursor molecules and reaction byproducts, followed by the introductionof the second precursor, or co-reactant, depicted as Pulse B, finalized by another purge step. This cycle is repeated until the desired thickness is obtained. 4

Figure 1.2 — Schematic of a regular ALD process, denoted by (a) and an ALD super-cycle, denoted by (c). The super-cycle can be divided into two binary cycles, the first being repeated m times and the second being repeated n times, until the desired film is produced. This schematic was adapted from [23]. 5

Figure 1.3 — Simplified representation of the typical ALD process for ZnO, on the left, and Al_2O_3, on the right. In the Al_2O_3 ALD process it can be seen that it is possible for the aluminum precursor to bond to either one or two surface sites, changing the number of reaction sites for the following step and, as a result, affecting the GPC 6

Figure 3.1 — ZnO thin film growth as a function of substrate temperature for different DEZ pulse times 11

Figure 3.2 — FTIR spectra of ALD-deposited ZnO films produced using different substrate temperature 12

Figure 3.3 — a) FTIR spectra of pure DEZ, b) FTIR spectra of a zinc-based metal organic framework, c) and d) FTIR spectra of this framework with different ammounts of DEZ. Adapted from [30] 13

Figure 3.4 — FTIR spectra of ALD-deposited AZO films compared to an undoped ZnO sample produced using the same deposition parameters 14

Figure 3.5 — Relationship between the Al content in AZO films with DEZ/TMA ratio. 15

Figure 3.6 — SEM mapping images of AZO thin films produced using different DEZ/TMA ratios. . 16

Figure 3.7 — GIXRD spectra for AZO films with four different DEZ/TMA ratio. 17

Figure 3.8 — Electrical properties of ZnO films using a DEZ pulse time of 0.5s in respect to substrate temperature........ 19

Figure 3.9 — Electrical properties of AZO films for different Al concentrations. a) film resistivity, b) Hall mobility, c) Carrier concentration and d) Hall mobility of undoped vs doped ZnO 19

Figure 3.10 — Variation in elemental composition of AZO films in regard to DEZ/TMA ratio 20

Figure 3.11 — XPS spectra of ALD-deposited AZO films: a) Zn 2p peaks; b) O 1s peaks; c) Al 2p peaks; d) Zn 3s peaks 21

Figure 3.12 — XPS spectra of the Zn Auger emission in ALD-deposited ZnO films with an Al_2O3 overlayer........ 21

Figure 3.13 — XPS spectra of Zn 3s and Al 2s obtained with the aid of CASAXPS........ 22

Figure 3.14 — Fitting used to determine the substrate/overlayer sensitivity factors using a) an X-ray source and b) an Ag X-ray source........ 23

Figure 3.15 — Change in Al_2O_3 overlayer thickness using different X-ray sources compared with ellipsometry data 23
Figure A1 — Thickness variation in AZO films as a function of DEZ/TMA ratio. A similar trend is observed for both water injection times. 37
Figure A2 — XRD measurements performed under a typical XRD configuration 37
Figure A3 — XPS spectra of all $ZnO+Al_2O_3$ samples deposited for this analysis 38
Figure A4 — Variation of the overlayer GPC as the number of cycles increases 38

LIST OF TABLES

Table 1 — Overview of existing literature in respect to the deposition of AZO films and their respective electrical and optical properties. 7
Table 2 — ALD pulse times used for the production of ZnO thin films. 9
Table 3 — ALD pulse times used for the production of AZO thin films 10
Table 4 — Elemental composition of AZO films as a function of DEZ/TMA ratio 14
Table 5 — Electrical properties of undoped and doped ZnO as a function of Al concentration. 18
Table 6 — Overlayer thickness of the ZnO+Al_2O_3 thin films determined with ellipsometry 23
Table 7 — Comparison between the expected and real thickness of AZO thin films 24

ACRONYMS

CENIMAT	Centro de Investigação de Materiais
i3N	Institute for Nanostructures, Nanomodelling and Nanofabrication
CEMOP	Centro de Excelência de Optoeletrónica e Microeletrónica de Processos
ALD	Atomic Layer Deposition.
CVD	Chemical Vapor Deposition
TCO	Transparent conducting oxides
ZnO	Zinc oxide
AZO	Aluminum-doped zinc oxide
DEZ	Diethylzinc
TMA	Trimethylaluminum
ITO	Indium tin oxide
GPC	Growth per cycle
FTIR	Fourier-transform infrared spectroscopy
SEM	Scanning Electron Microscopy
EDS	Energy-dispersive X-ray spectroscopy
XRD	X-ray diffraction
GIXRD	Grazing incidence X-ray diffraction
XPS	X-ray photoelectron spectroscopy

Symbols

ρ	Resistivity
μ	Carrier mobility
Å	Angstrom
Al	Aluminum
Ag	Silver
$Zn(C_2H_5)_2$	Diethylzinc
$Al(CH_3)_3$	Trimethylaluminum

MOTIVATION AND OBJECTIVES

Transparent conducting materials (TCMs) are a technological necessity in several industries, mainly due to their distinctive ability to combine notable electrical conductivity with high transparency within the visible range. Among these materials, several candidates have rose to prominence and have seen substantial research, such as metal meshes and metallic nanowire networks (MNWs) that are able to be produced in a low-effort, cost-efficient fashion and, most importantly, they are entirely compatible with large area deposition techniques [1]. Besides these previous examples, carbon-based materials have also attracted much attention, namely carbon nanotube networks (CNTs) and single layer graphene, with the latter being able to exhibit extraordinary carrier mobilities while also achieving very high optical transmittance [2]. However, graphene does have its own shortcomings, and even though several methods to deposit graphene exist, the rather complex nature of these processes has resulted in rather low output volumes, accompanied by very high production costs, making it extremely difficult to utilize this material to its full capacity in an industrial setting.

Historically speaking, and despite the promising results obtained with the materials discussed above, transparent conducting oxides (TCOs) have become the dominant and most commonly used TCM, witnessing a rise in popularity with the emergence of flat-panel displays [2], a consequence of their superior properties, with the most common being indium-doped tin oxide (ITO). Nevertheless, ITO has also seen a decrease in popularity due to issues regarding the general availability and sustainability of indium, leading to the research and development of alternative oxides, such as doped zinc oxide (ZnO), which can be deposited using a variety of fabrication techniques. One possible production method is atomic layer deposition (ALD), a surface-controlled, vapor phase variant of the chemical vapor deposition technique (CVD), that offers some major advantages, such as the ability to deposit highly conformal and uniform films across a given substrate [3].

Within this context, the major objectives of this work were the establishment of an optimized ALD process capable of depositing ZnO thin films using low substrate temperatures, <200 ºC, and the evaluation of the effect of dopant concentration (aluminum) on the electrical, morphological and chemical properties of these films, in order to produce TCOs capable of competing with the current market. By accomplishing these goals, not only would it be possible to consistently produce TCO-based technologies at CENIMAT|i3N/CEMOP, but it would also solidify the ALD technique as a suitable deposition method for future applications.

This work received funding from the European Community's H2020 program under grant agreement no. 716510 (ERC-2016-StG TREND), no. 951774 (FOXES) and H2020 Synergy (GA 952169).

1 INTRODUCTION

This chapter serves as an introduction to the different notions required to understand the present work, not only regarding the basic understanding of TCO film technology and operation, but also the fabrication techniques employed to produce said films.

1.1 Transparent conducting oxides (TCOs)

Transparent conducting oxides (TCOs) encompass a rather distinct class of materials that are able to consolidate high optical transparency in the visible range with high electrical conductivity [4], [5]. These appealing properties have, naturally, led to the extensive research, development and subsequent implementation of said materials in a multitude of applications and industries, such as displays, optoelectronics and transparent devices, just to name a few [4]–[6]. Additionally, given the ever-growing need for renewable and efficient energy sources, TCOs have also seen substantial use in smart windows and photovoltaic devices [5].

Indium tin oxide (ITO) is a wide optical band-gap material (3.7 eV) with low electrical resistivity and high optical transparency [6] and, as a result, it has been the most commonly used TCO, accounting for approximately 90% of all indium consumption worldwide [7]. However, despite the aforementioned qualities, ITO does possess its own shortcomings, such as chemical instability under certain processes which could limit its applications [6], toxic effects on humans [6], with studies using animal trials indicating that exposure either through inhalation or ingestion of indium and some of its compounds could lead to hazardous effects on the lungs, heart and kidneys [8]–[10], especially during the mining process. Last but definitely not least, the scarcity of indium serves as one of the main obstacles in regard to achieving a sustainable, economically-viable, long-term production of TCO-based technologies [6][11]. This is mainly due to two different factors, firstly, the fact that indium is obtained solely as a by-product of other mineral deposits [12] and, therefore, its supply is intrinsically linked to the efficiency of the extraction processes and economical markets of said ores, making ITO a high processing cost material. Secondly, the fact that most indium production is confined to a few select countries, leading to a rather lack of transparency in terms of indium availability and susceptibility to harsh export quotas, severely impacting the international markets [12], [13]. With these issues in mind, the research and development of indium-free alternatives is of upmost importance.

1.1.1 AZO: A suitable alternative

Zinc oxide (ZnO) is an incredibly popular semiconductor material due to its versatile nature and low processing cost. It is an n-type material with a wide band gap of approximately 3.2 eV at room temperature, high chemical stability and a free electron concentration of up to 10^{20} cm^{-3} [6][14]. In a similar fashion to ITO, these properties have put it in the spotlight as a worthy contender for TCO applications, especially when doped with different impurities, such as Ga (GZO), F (FZO) and, as the purpose of this work implies, Al (AZO) [14], with the latter allowing a considerable decrease in film resistivity, depending on dopant concentration, in order to obtain similar electrical properties to those of ITO, with some reports achieving values of 7.60×10^{-4} [15], 5.1×10^{-4} [16] and 8.54×10^{-5} Ω*cm [17], when depositing films on glass substrates using DC sputtering, RF sputtering and pulsed laser deposition (PLD), respectively. As can be seen, the properties of AZO films vary based on the production method employed and, as such, it is crucial to utilize a technique that allows for the deposition of films with good electrical, morphological and optical qualities on cost-effective, long area substrates.

1.2 Atomic Layer Deposition (ALD)

Atomic Layer Deposition (ALD) is a surface-controlled, vapor phase technique that enables the production of thin films using a vast array of materials [3], with the first ALD process of a ZnS system being successfully demonstrated in the 1970s, initially called Atomic Layer Epitaxy (ALE), by finnish researcher Tuomo Suntola and his team, with subsequent research, led by Nishizawa, demonstrating the ability to deposit GaAs thin films in the 1980s [18], [19]. Its current denomination however, only became more common in the early 2000s [18][20].

ALD is considered as a special variant of the chemical vapor deposition (CVD) technique given the use of gaseous reactants, also known as precursors, in order to form the desired films via chemical surface reactions [21]. Despite these similarities, ALD does possess distinguishable advantages when compared to other deposition methods, such as the aforementioned CVD, and/or physical vapor deposition (PVD) techniques, namely a greater control over film thickness, composition and overall conformality, while also allowing depositions conducted at modest temperatures (<350 ºC) [3], facilitating film production on top of flexible, temperature-sensitive polymeric/plastic-based substrates. As a result, ALD has solidified itself as a mainstream tool, especially in the semiconductor industry, where the increasing device miniaturization and development of high-aspect-ratio structures require an atomic level control of coatings/films [20], [21].

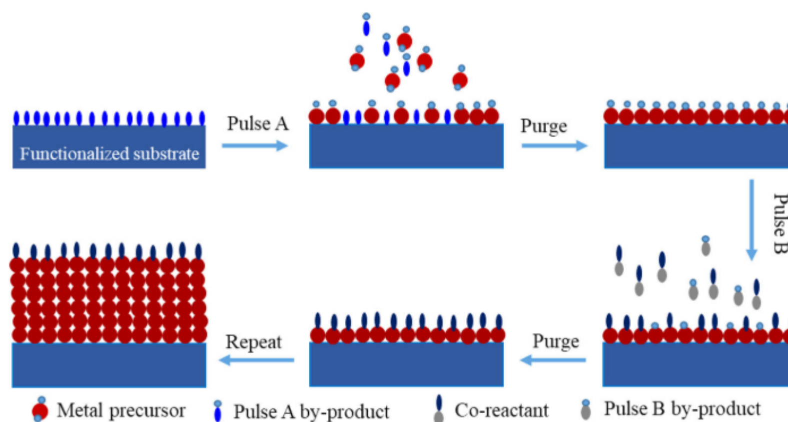

Figure 1.1. Illustration of a typical ALD cycle. In this process, a metallic precursor is introduced into the chamber, depicted through Pulse A. After all surface functional groups have reacted with this precursor, a purge step removes all unreacted precursor molecules and reaction byproducts, followed by the introduction of the second precursor, or co-reactant, depicted as Pulse B, finalized by another purge step. This cycle is repeated until the desired thickness is obtained [47].

These advantages pertain to the idiosyncratic behavior of ALD, shown in Figure 1.1, where precursor gases are pulsed, individually and alternately, unlike its CVD counterpart, into a chamber, separated by purge steps using an inert gas in order to prevent gas phase reactions and subsequent contaminations [21]. These alternating cycles ensure that, in theory, only surface reactions occur given the limited amount of reactive surface sites, leading to a self-limiting behavior, i.e., the deposition of individual, ultra-thin atomic monolayers. These monolayers are then stacked on top of each other and based on the number of cycles, lead to the formation of a film with, as previously stated, a well-controlled thickness and a specific rate of film growth, typically known as growth per cycle (GPC). Nonetheless, specific conditions must be met in order to achieve a stable GPC, those of which can vary depending on precursor species, oxidant species, the pulse times during each cycle and, perhaps most important in a traditional ALD process, the substrate's temperature, that will provide the necessary energy to facilitate all reactions between precursors and surface sites, hence this

technique's formal classification of thermal ALD. Ergo, finding an adequate process temperature located within what is called the temperature window, a temperature interval in which optimal growth is obtained without jeopardizing the ideal ALD behavior, either due to precursor condensation/decomposition or surface desorption, is required.

Conversely, plasma enhanced ALD (PEALD) differs from thermal ALD by using plasma as a reactant and as the main reaction energy source [22], with the highly reactive radicals created by a plasma source allowing for depositions at lower temperatures, with a higher growth rate when compared to its counterpart [23]. Even though this specific technological branch started as a niche method to expand the already well understood capabilities of ALD, it enabled high-volume manufacturing and can be considered as a large field of study in of itself [16]. A different variant, concomitant to both the traditional and plasma variations of this technique is the Spatial ALD that, when compared to its counterparts, provides a far more efficient use of precursor gases due to its distinct configuration, making it extremely appealing in large scale applications and roll-to-roll processes [24].

1.2.1 ALD of ZnO/AZO

Even with the basic principles of this technique explained in the previous point, it is important to fully understand the mechanisms and reaction kinetics that occur between the precursors necessary to produce both ZnO and AZO films. Concerning the former, a cyclic repetition of a zinc precursor pulse, the most commonly reported and well-studied being diethylzinc (DEZ), alongside a co-reactant/oxidant species, such as hydrogen peroxide, H_2O_2, ozone, O_3 or, as the purpose of the present work entails, water, H_2O, is required. With this premise in mind, it is safe to classify this process as a regular/binary ALD cycle [20].

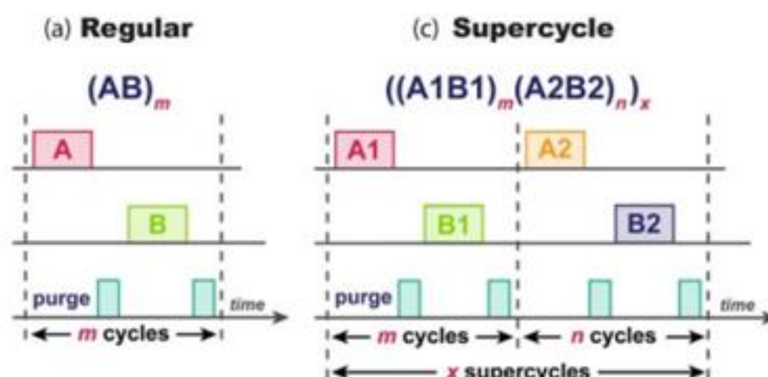

Figure 1.2. Schematic of a regular ALD process, denoted by (a) and an ALD super-cycle, denoted by (c). The super-cycle can be divided into two binary cycles, the first being repeated m times and the second being repeated n times, until the desired film is produced. This schematic was adapted from [26].

AZO, however, is a doped material and, therefore, the introduction of an aluminum oxide precursor is needed, with trimethylaluminum (TMA) being the most common due to its simple chemistry and well understood reaction kinetics. Given the use of an additional chemical species we can consider the ALD process of AZO as alternating cycles of two binary ALD processes, that of ZnO and that of Al_2O_3, in what is described as a super-cycle [25]. By changing the number of individual binary cycles in respect to each other, a ternary film can be produced with varying doping concentrations [25], [26]. A simple schematic can be seen in Figure 1.2., differentiating both binary and ternary ALD cycles.

With this distinction in mind, here follows a simple overlook on the chemical reactions that occur during the deposition of these two oxides, with the following equations, alongside Figure 1.3., serving as an effective representation of the ALD sub-cycles required to deposit ZnO, equations (1.1) and (1.2), and AZO, equations (1.1), (1.2), (1.3) and (1.4), on a Si substrate.

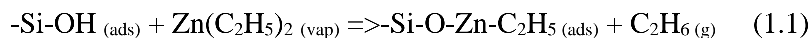

$$-Si\text{-}OH_{(ads)} + Zn(C_2H_5)_{2\,(vap)} \Rightarrow -Si\text{-}O\text{-}Zn\text{-}C_2H_{5\,(ads)} + C_2H_{6\,(g)} \quad (1.1)$$

$$-Si\text{-}O\text{-}Zn\text{-}C_2H_{5\,(ads)} + H_2O_{(vap)} \Rightarrow -Si\text{-}O\text{-}Zn\text{-}OH_{(ads)}{}^{*} + C_2H_{6\,(g)} \quad (1.2)$$

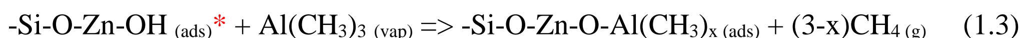

$$-Si\text{-}O\text{-}Zn\text{-}OH_{(ads)}{}^{*} + Al(CH_3)_{3\,(vap)} \Rightarrow -Si\text{-}O\text{-}Zn\text{-}O\text{-}Al(CH_3)_{x\,(ads)} + (3-x)CH_{4\,(g)} \quad (1.3)$$

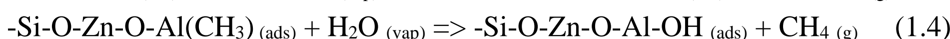

$$-Si\text{-}O\text{-}Zn\text{-}O\text{-}Al(CH_3)_{(ads)} + H_2O_{(vap)} \Rightarrow -Si\text{-}O\text{-}Zn\text{-}O\text{-}Al\text{-}OH_{(ads)} + CH_{4\,(g)} \quad (1.4)$$

In equation (1.1), the zinc precursor is introduced into the ALD chamber and, if the right conditions are met, it reacts with the substrate's surface sites, with the release of one of its ethyl groups. After the removal of the unwanted chemical byproducts, the co-reactant, water, is introduced, leading to the substitution of the remaining ethyl group, as seen in (1.2). The repetition of these two equations should, therefore, result in the formation of a uniform ZnO film. However, if the deposition of AZO is desired, the addition of equations (1.3) and (1.4) is required. Equation (1.3) portrays the introduction of the aluminum precursor right after the purge that succeeded (1.2), bonding directly to the available OH groups and releasing one methyl group. After the removal of this methyl, water is directly incorporated onto the film, as seen in (1.4). Depending on the intended dopant concentration, the number of cycles of equations (1.3) and (1.4) must be carefully devised.

This short explanation should be taken as exactly what it is, a simple summary, given that other factors such as precursor thermodynamical preferences or steric hindrances could affect film growth [18][26], [27]. In the future, the study of these contributions could be of significant interest.

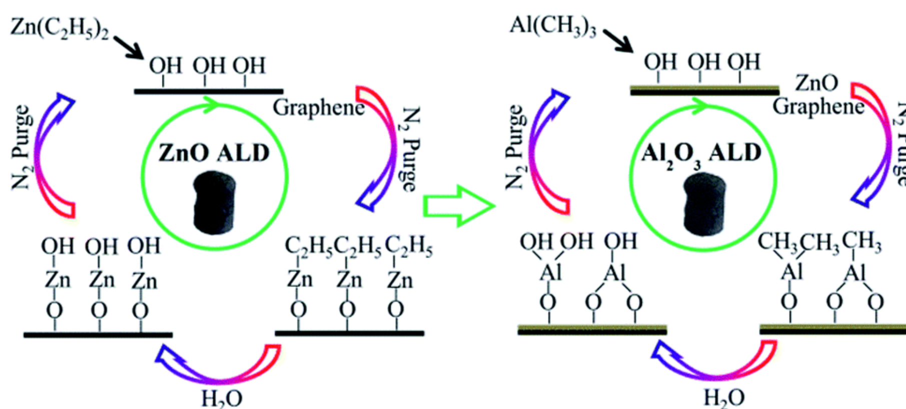

Figure 1.3. Simplified representation of the typical ALD process for ZnO, on the left, and Al_2O_3, on the right. In the Al_2O_3 ALD process it can be seen that it is possible for the aluminum precursor to bond to either one or two surface sites, changing the number of reaction sites for the following step and, as result, affecting the GPC [28].

1.2.2. AZO: A literary overview

As mentioned in point 1.1.1, AZO can serve as a promising alternative to the more conventional indium-based oxides that are used to produce TCOs. As such, plenty of research has been made in order to study and optimize the properties of this oxide, with the following Table 1 serving as a small overview of some of the existing literature in regard Al-doped ZnO. This academic survey will, therefore, provide an important framework with which to compare the results shown in the following sections.

Table 1.Overview of existing literature in respect to the deposition of AZO films and their respective electrical and optical properties

					Electrical properties			Optical properties	
Deposition technique	Zn precursor	Al precursor	Co-reactant	Temperature (ºC)	Resistivity (Ω*cm)	Carrier concentration (cm^{-3})	Mobility ($cm^2/V*s$)	Transmittance (%)	Ref.
ALD	DEZ	TMA	H_2O	200	$1.7x10^{-3}$ – $3.2x10^{-3}$	$1.4x10^{20}$ – $4.7x10^{20}$	7.6 - 14.3	–	[4]
				150	$5.84x10^{-4}$	–	–	~90	[29]
				150	$1x10^{-2}$	$\sim10^{20}$	3	80 – 85	[6]
				160	$6.63x10^{-3}$ – $9.98x10^{-2}$	$7.7x10^{18}$ – $1.34x10^{20}$	1.33 – 16.4	–	[14]
				200	$7x10^{-4}$ – $1.2x10^{-3}$	$3.6x10^{20}$ – $5.1x10^{20}$	15 – 21.8	~90	[30]
PLD	Doped ZnO target		-	165-300	$8.54x10^{-5}$	$1.54x10^{21}$	47.6	83	[17]
Pulsed DC Magnetron Sputtering			-	RT	$1.7x10^{-3}$	$2.6x10^{20}$	13.6	73	[16]

2 Materials and Methods

This section's main purpose is to introduce the main fabrication and deposition techniques employed during the course of this work, in order to adequately characterize the samples that were produced.

2.1 Thin film deposition

Silicon wafers and 2.5x2.5 cm Corning Eagle glass were used as substrates for the deposition of ZnO and AZO films. These substrates were subjected to the exact same cleaning process, i.e., a 10 minute ultrasonic bath in acetone in order to remove any organic contaminants, followed by a second ultrasonic bath, this time in isopropanol, while still maintaining the same duration. The main purpose of this bath was to eliminate any acetone residue still left on the substrates. Afterwards, both glass and silicon wafers were cleaned with ultra-pure water and subsequently dried with the aid of a nitrogen gun. In order to remove surface moisture, these substrates were placed on a hot plate, where they would remain undisturbed for 20 minutes at a temperature of 120 ºC. Although the cleaning process is complete, the substrates were submitted to a final nitrogen spray prior to every deposition.

In regard to the oxide depositions, a Beneq TFS-200 reactor was employed, with diethylzinc (DEZ), trimethylaluminum (TMA) and water being used, with the first two serving as the metallic precursors, while the latter served as the oxidant species. Five different temperatures were used to deposit ZnO films, ranging from 100 ºC up to 200 ºC, with a step of 25 ºC, in order to assess the dependency of electrical and morphological film properties with substrate temperature. The AZO films on the other hand, were only deposited at a temperature of 150 ºC, for reasons that will be revealed later on this work. The recipes used are fully disclosed in Table 2, Table 3, Annex 1 and Annex 3. Following the ALD depositions, aluminum contacts were deposited on the ZnO/AZO films produced on top of the glass substrates using a home-made e-beam evaporation system, for subsequent electrical measurements. Four-terminal configurations were produced, always using shadow masks for electrode pattern definition and a deposited thickness of 100 nm.

Additional ZnO/AZO films were prepared in order to assess the interface behavior between ZnO and Al_2O_3. As such, four separate ZnO films were produced on the same substrates as the films described previously, all following the same recipe and using the same substrate temperature. Al_2O_3 of varying thickness was then deposited on top of three of these films, following the recipe seen in Annex 2, with the fourth being left untouched in order to serve as reference. This was meant to analyze the effect of the aluminum-based oxide on the underlying ZnO film and see how the initial growth of the former could be affected.

Table 2. ALD pulse times for the production of ZnO thin films

Sample	Temp. (ºC) Step:25 ºC	DEZ pulse (s)	DEZ purge (s)	H_2O pulse (s)	H_2O purge (s)	Nº of ZnO cycles
ZnO T2	100-200	2				
ZnO T3	100-200	1				
ZnO T4	100-200	0.5	8	3	4	200
ZnO T5	100-200	0.250				
ZnO T6	100-200	0.125				

Table 3. ALD pulse times used for the production of AZO thin films.

Sample	Temp. (°C)	DEZ/TMA ratio	TMA pulse (s)	TMA purge (s)	H_2O pulse (s)	H_2O purge (s)	N° of Al_2O_3 cycles
AZO 1:1	150	1	0.15	5	0.5	4	200
AZO 2:1		2					100
AZO 5:1		5					40
AZO 10:1		10					20
AZO 20:1		20					10
AZO 50:1		50					4
AZO 100:1		100					2
ZnO T4	150	-	0	0	3	4	0
XPS 1	150	-	0.15	5	0.5	4	1
XPS 20							20
XPS 40							40

Note 1: The zinc pulse times employed here were those used in ZnO T4, however, due to time constraints, the water pulse time of the ZnO half-cycle was lowered from 3 to 0.5 s, with negligible difference in GPC (Annex 4), hence its exclusion from this table, as to avoid redundancy.

2.2. Thin film characterization

A Biorad/Nanometrics HL5500 Hall effect system was utilized in order to study film bulk resistance, resistivity, carrier concentration and carrier mobility of ZnO/AZO samples on glass with four-terminal configuration (Van der Pauw).

The samples deposited on top of silicon wafers were submitted to FTIR and thickness analysis using a Thermo Nicolet 6700 and a Horiba-Jobin Yvon spectroscopic ellipsometer, respectively. This study would, therefore, provide crucial information in regard to the oxide's behavior and growth kinetics during deposition and make it possible to ascertain if the samples were indeed produced under an effective ALD regime with a stable growth per cycle (GPC).

Given the differing aluminum concentration in the AZO films, a change in crystallinity was to be expected and, as such, the AZO samples of ratio 100:1, 10:1, 2:1 and 1:1 were submitted to XRD and GIXRD measurements. These tests were performed with the aid of a PANalytical Xpert PRO, employing a Cu K-alpha source of λ=1.540598 Å. Given the nature of the GIXRD configuration, a small incident angle, ω, of 0.5° was fixed. This technique would provide a surface sensitive spectra that could directly state the effect of the aluminum atoms on the naturally crystalline structure of ZnO.

Last but not least, XPS measurements were also performed on the four ZnO/Al_2O_3 samples specifically deposited for this effect. By using a Kratos Axis Supra with monochromatic Al Kα radiation and an analyzer pass energy of 10 eV , the chemical composition of both the ZnO "substrate" and Al_2O_3 overlayer were investigated, with the main purpose being the observation of the characteristic peaks of both species and how these would change according to the increasing overlayer thickness. Besides, XPS analysis was also used to extrapolate film thickness and, as a direct result, film GPC, using a quantitative study that would compare specific Zn/Al orbital intensities. This approach, although not incredibly precise, could indicate if there were any underlying mechanisms that could jeopardize the film conformality and uniformity associated with the ALD process.

3. RESULTS

The following section intends to shed some light on the properties of the undoped and doped ZnO thin films that were produced using the process parameters stipulated above. Understanding the morphological, electrical and chemical behavior of these samples is, therefore, of paramount importance in order to optimize the production of ALD-deposited conducting oxides.

3.1. Film Growth, morphology and elemental analysis

3.1.1 Ellipsometry

The growth of ZnO and AZO thin films was measured with the aid of an ellipsometer, in order to determine the effect of substrate temperature and precursor pulse time on their thickness and GPC, with Figure 3.1 aptly addressing the question regarding the undoped films. It is readily apparent that, in the temperature range of 125-150 ºC, typical ALD behavior is achieved for precursor injection times above 0.5 s (solid lines), with a constant thickness and GPC being obtained inside said interval. As expected, when employing lower precursor injection times (dotted lines), ZnO thin films were not able to attain GPC stability in any given temperature range, simply due to the limited quantity of DEZ, which is unable to cover the entire substrate area and form a uniform monolayer.

Additionally, Figure 3.1. also states the clear effect of substrate temperatures outside the previously mentioned ALD window on film growth behavior. Samples produced below this interval possess a lower GPC, attributed to the insufficient thermal energy, leading to a lack of surface site reactions with the precursor/co-reactant. Similarly, the deposition of ZnO above this optimal thermal range also leads to an inhibited GPC, however, unlike previously, this might be due to either temperature-promoted removal of surface reactive sites or precursor desorption, with both mechanisms being known to inhibit film growth [26]. Additionally, it is important to note that the interval in which thin films are able to steadily grow regardless of substrate temperature is entirely dependent on the precursor species that are used, with the present results being in agreement with the existing literature, since DEZ is known to have a characteristic ALD window anywhere between the temperatures of 100 up to 170 ºC [31].

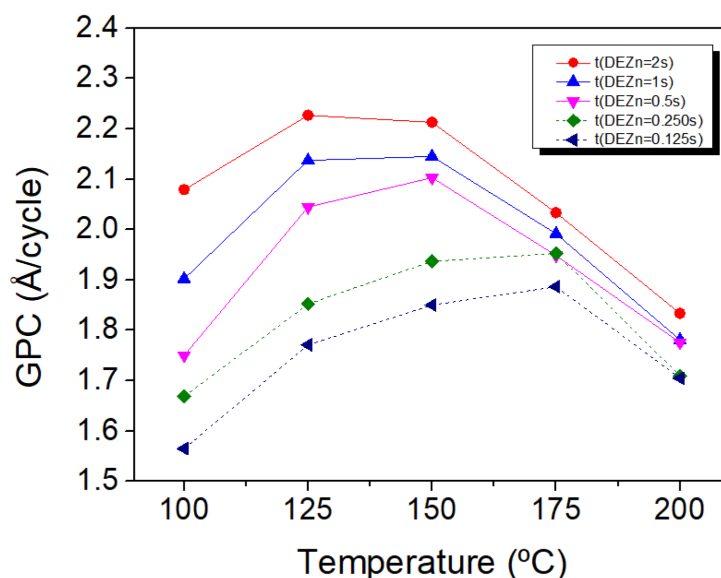

Figure 3.1. ZnO thin film growth as a function of substrate temperature for different DEZ pulse times

In accordance with the previous observations, all subsequent depositions were made using a substrate temperature of 150 ºC alongside a DEZ pulse of 0.5 s. According to Figure 3.1, a higher pulse time would indeed seem to better fit the ALD regime. The original intention was, however, to study the effect of two different precursor pulse times, 0.5 and 2 s, on film properties but, due to time constraints, that proved to be unfeasible, with only the study of the former being undertaken.

3.1.2. FTIR

FTIR-ATR measurements were performed on samples produced using the aforementioned deposition parameters, in order to gauge the effect of an increasing Al content on ZnO films. Nonetheless, the infrared response of undoped ZnO was first carried out in a wide range of temperatures. Even though all AZO films were deposited using a fixed substrate temperature, this analysis served as an indicator to see if any precursor decomposition occurred and/or if the precursor species would remain in the films due to non-optimal purge times. In Figure 3.2. a noticeable peak can be seen around 1110 cm^{-1}, traditionally attributed to the Si-O bond, which is perfectly understandable given the fact that the films were deposited on silicon substrates. However, due to the relatively small film thickness, some equipment artifacts were present in the FTIR spectra, particularly for smaller wavenumbers and, as such, all data below a wavenumber of 750 cm^{-1} had to discarded. As a result, the characteristically intense Zn-O stretching vibration whose peaks are typically located between 400-420 cm^{-1} [32] cannot be seen, making it impossible to evaluate the effect of substrate temperature on the bonds between oxygen and the metallic ions. Nevertheless, there is some information that can be extracted from this spectra, namely the non-existence of peaks for wavenumbers between 2900-3000 cm^{-1}, associated with the stretching modes of the C-H bond [33], indicates that no organic precursor byproduct, ethane in the case of the ZnO ALD process, is incorporated into the film.

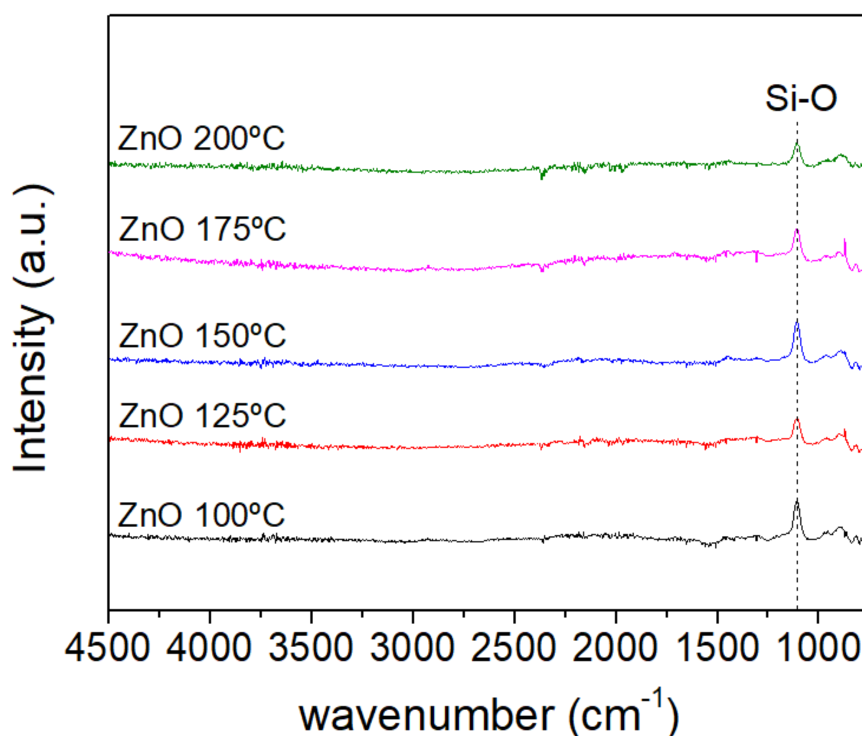

Figure 3.2. FTIR spectra of ALD-deposited ZnO films produced using different substrate temperatures

As a point of reference, Figure 3.3. shows the change in infrared response of a microporous zinc-based framework with the introduction of DEZ, with a) presenting the FTIR spectra of this metallic precursor [34]. Even though the deposition technique employed by the research group responsible for this study, MOCVD, was different than the one used in this work, it still proves the clear existence of C-H bonds in the exact same wavenumber region as mentioned before, highlighted in yellow. Thus, it is possible to remove any possible doubt that, during the ALD process, organometallic precursor decomposition occurs.

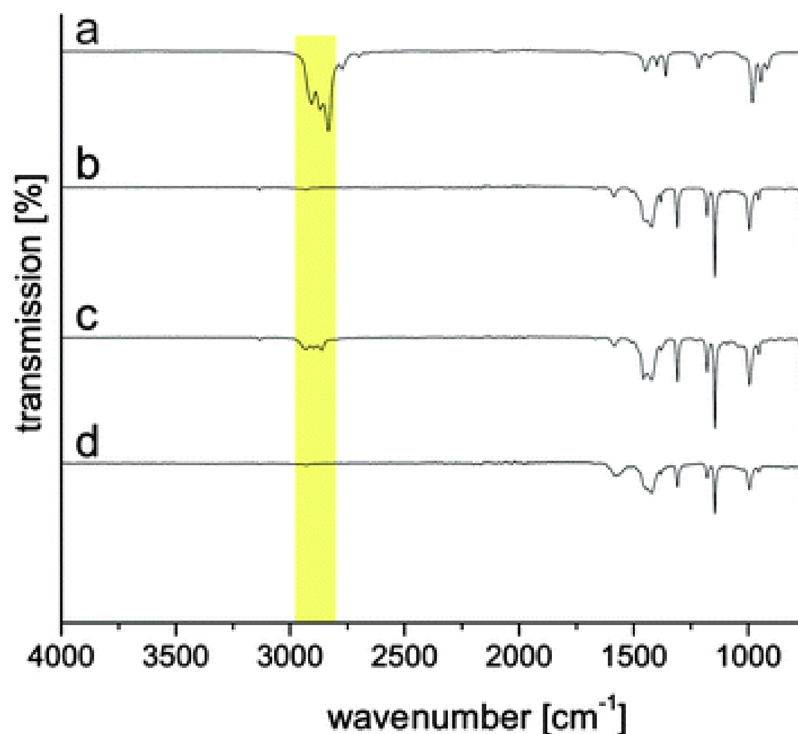

Figure 3.3. a) FTIR spectra of pure DEZ, b) FTIR spectra of a zinc-based metal organic framework, c) and d) FTIR spectra of this framework with different amounts of DEZ. Adapted from [30].

With the infrared study of undoped ZnO concluded, only the AZO films remained to be analyzed. Figure 3.4. displays the FTIR data obtained for all AZO films and compares them with the spectra of ZnO deposited using the same temperature. Just like in Figure 3.2., lower wavenumbers were disregarded and, just like previously, it resulted in the loss of the Zn-O peak, preventing the evaluation of the effect of dopant introduction on this bond.

The majority of the AZO films have an infrared response very similar to that of its undoped counterpart. However, for the two samples deposited using the lowest DEZ/TMA ratios, a rather broad peak located around 850-900 cm^{-1} emerged, a direct result of the stretching of the Al-O bond [35]. Given the fact that this seems to be the case for only the two most Al-rich samples, this points out that the introduction of great amounts of Al ions into the ZnO structure promotes the formation of an Al_2O_3 lattice. The absence of the Al-O peak for lower doping indicates that extended Al-O lattice structures are not present since these are the prerequisite for the characteristic dipole moment of Al_2O_3. Therefore, when individual substitution of Zn by Al occurs, the neighboring oxygen atoms are still shared with Zn (and not entirely Al), so the dipole moment has to be different when compared to an extended Al_2O_3 structure.

However, due to our inability to see the effect of doping in the intensity of the Zn-O peak, the way the Al is incorporated into the ZnO matrix is unclear and, therefore, other methods of film characterization should be taken into consideration.

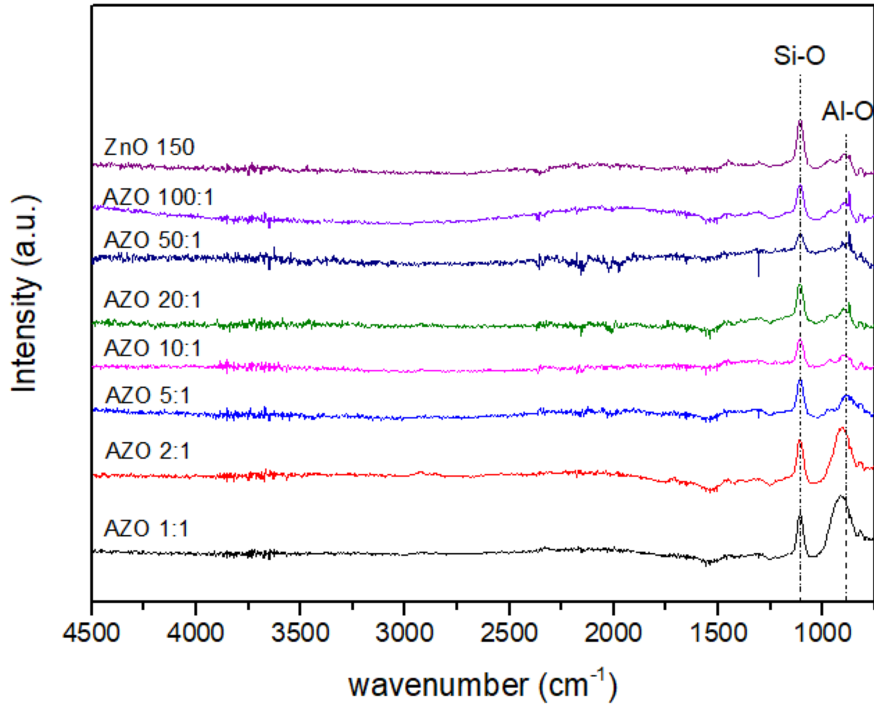

Figure 3.4. FTIR spectra of ALD-deposited AZO films compared to an undoped ZnO sample produced using the same deposition parameters.

3.1.3. SEM/EDS

Following the deposition of undoped ZnO, AZO films were deposited using the deposition parameters stated in the previous point. By changing the number of cycles of each metalorganic precursor, or simply put, the DEZ/TMA ratio, films with varying dopant concentration were produced. However, after this process was complete, an important question still remained, namely as to what extent was the success of the presented doping method in incorporating Al into the ZnO films. To find out, SEM-EDS analysis was performed in order to assess the dopant concentration, provided in Table 4 and Figure 3.5, in as-deposited AZO films.

This table corroborated the notion that the Al concentration was inversely proportional to the DEZ/TMA ratio but, unexpectedly, it revealed the complete domination and substitution of the Zn atoms in samples with lower precursor ratios.

Table 4. Elemental composition of AZO films as a function of DEZ/TMA ratio

	Sample						
	AZO 1:1	**AZO 2:1**	**AZO 5:1**	**AZO 10:1**	**AZO 20:1**	**AZO 50:1**	**AZO 100:1**
DEZ/TMA ratio	1	2	5	10	20	50	100
Al, At.%	35.49	31.44	14.86	7.14	3.89	2.42	1.98
Zn, At.%	9.58	16.12	36.72	46.63	50.47	52.23	52.49
O, At.%	54.93	52.44	48.42	46.22	45.64	45.35	45.54

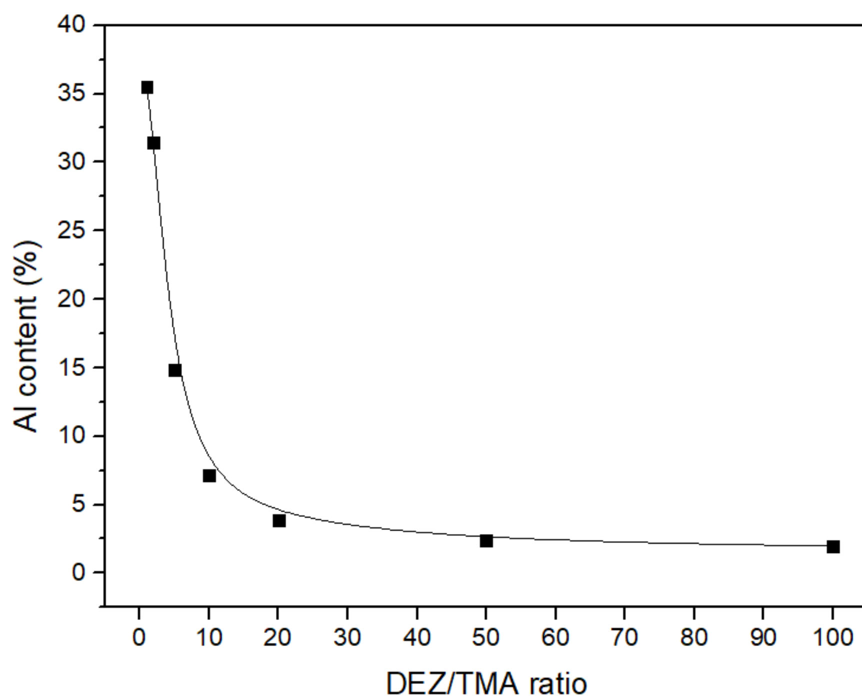

Figure 3.5. Relationship between the Al content in AZO films with DEZ/TMA ratio

This surge in dopant substitution could, in theory, cause lattice distortions that would severely impact both the crystallographic and electrical properties of AZO films. With that in mind, surface imaging was carried out on the samples AZO 1:1, AZO 2:1, AZO 50:1 and AZO 100:1, with the results being presented in Figure 3.6. As expected, the two lightly doped films do seem to present a rougher surface when compared to their counterparts, even showing the existence of small crystals, falling completely in line with the fact that ALD deposited ZnO tends be polycrystalline. On the other hand, the two remaining samples, AZO 1:1 and AZO 2:1 are completely flat and smooth, suggesting a more amorphous character, proving that as more aluminum is introduced the more frequently disturbed the ZnO growth is, inhibiting the formation of the typical polycrystalline structure. To prove this theory, the evaluation of the crystallographic changes in relation to dopant concentration had to be performed.

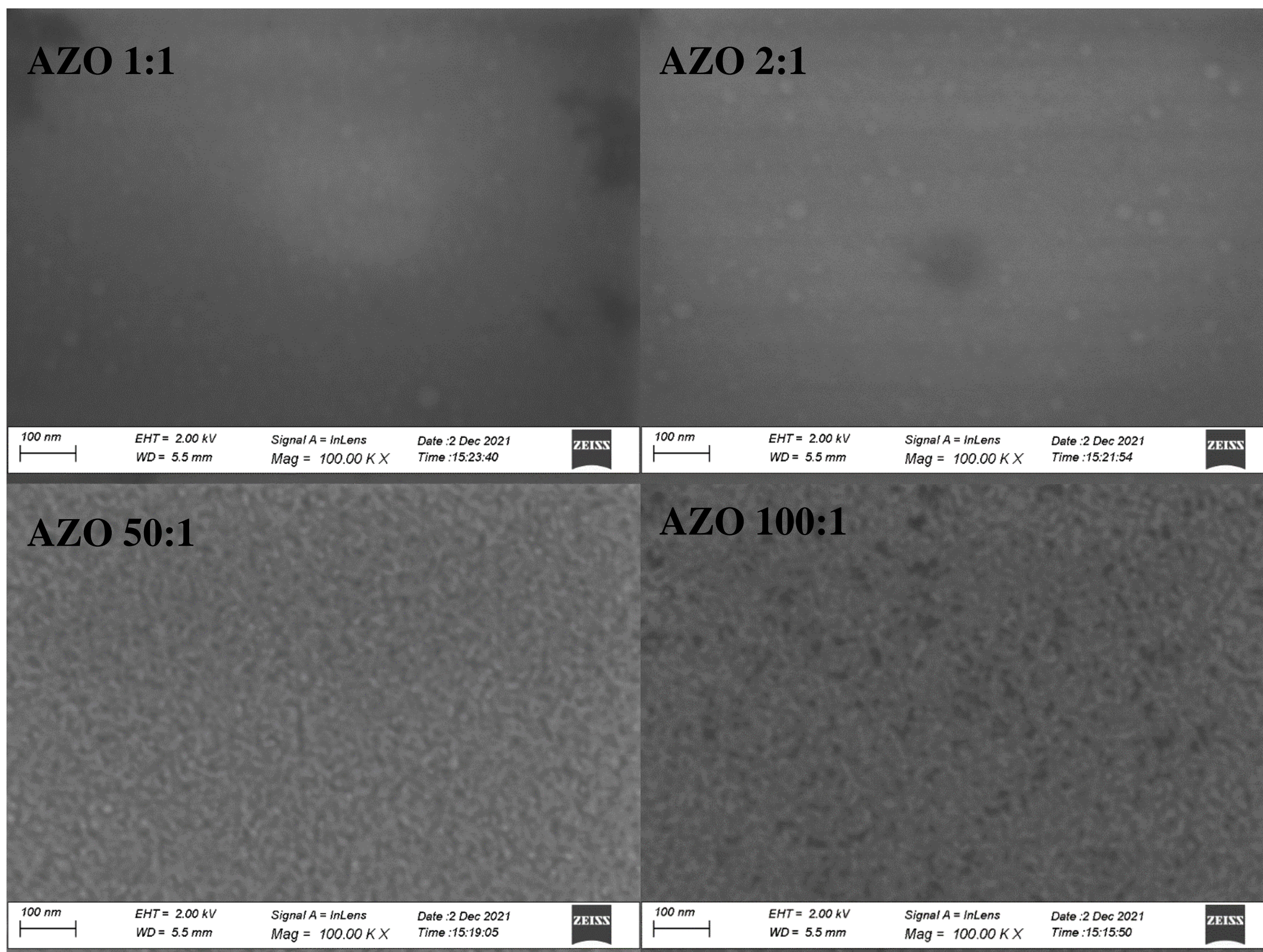

Figure 3.6. SEM mapping images of AZO thin films produced using different DEZ/TMA ratios

3.1.4. GIXRD

Figure 3.7. presents the GIXRD results performed on some of the AZO samples with the main intent of corroborating the previous statement regarding surface morphology and any possible lattice distortions induced by excessive dopant incorporation. These results demonstrate that AZO films produced using a DEZ/TMA ratio of 100:1 are polycrystalline, with the characteristic peaks typically attributed to the wurtzitic phase of ZnO being observed at 31.93º (100), 34.55º (002), 36.37º (101), 47.67º (102) and 56.79º (110), with the (002) direction being the most thermodynamically favorable orientation, as a result of the low surface energy of this crystalline plane [36]. However, as Al content increases, the films become progressively less crystalline, with the AZO 2:1 and AZO 1:1 being completely amorphous, a consequence of excessive lattice distortions. An interesting result was, however, the change of the preferred orientation in the AZO 10:1 sample where, despite retaining the characteristic ZnO peaks, (100) became the dominant orientation as opposed to the (002) seen in AZO 100:1. It is important to note that the (002) plane is comprised of alternating planes of Zn^{2+} and O^{2-} and, therefore, it is either positively or negatively charged, respectively, whereas the (100) plane is comprised of alternating rows of these same ions, resulting in the charge neutrality of this surface [6]. With the increase of Al^{3+} ions and subsequent random substitution of the lattice Zn, the surface charge of both these planes could have been affected and, ultimately, changed the preferential growth of this oxide.

Another point that must be taken into account is the clear presence of peaks in the range of 50-60º for all samples, which can be attributed to the silicon substrate. Due to the extremely low incident angle and the lack of a monochromator, some of the X-ray beams were able to hit the substrate's lattice planes in such a way that it resulted in the appearance of a silicon-based signal. This does not seem to jeopardize the analysis of the samples but, even so, the films were also analyzed under the normal XRD configuration, which can be seen in Annex 5, providing the same results without any substrate interference.

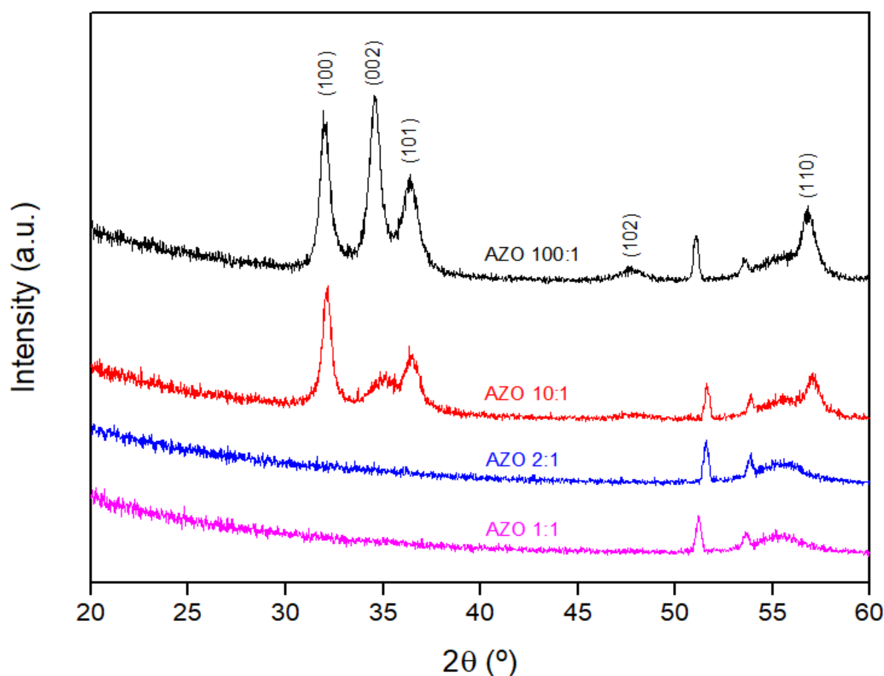

Figure 3.7. GIXRD spectra for AZO films with four different DEZ/TMA ratios

3.2. Electrical properties

3.2.1. Hall measurements

Following the deposition of metallic contacts, the ZnO and AZO films were electrically characterized as to ascertain the effect of dopant concentration on film resistivity and carrier mobility/concentration, when compared to undoped films. Starting with the former, the use of different substrate temperatures clearly had an impact on the electrical qualities of ZnO films (Figure 3.8. and Table 5). The data conveys that, as temperature increases from 100 to 150 ºC, film resistivity drastically decreases from 1.83×10^{4} to 3.81 Ω*cm, while carrier concentration increases from 1.96×10^{14} to 3.84×10^{19} cm^{-3}, all this accompanied by a reduction in Hall mobility, from 1.78 to 0.77 cm^{2}/V*s. Generally speaking, an increase in carrier concentration is accompanied by a rise in charge scattering, ultimately decreasing mobility [37], which could explain this behavior. On the other hand, films deposited at a temperature of 200 ºC not only saw an even greater decrease/increase in film resistivity/carrier concentration, from 3.81 to 7.08×10^{-3} Ω*cm and 3.84×10^{19} to 1.21×10^{20} cm^{-3}, respectively, but also an improvement in Hall mobility, from a measly 0.77 to 7.33 cm^{2}/V*s, an increase of almost tenfold. This might come as a result of improved film crystallinity, induced by a higher substrate temperature, which could have been absent from the samples deposited at lower temperatures.

Table 5. Electrical properties of undoped and doped ZnO as a function of Al. concentration

Sample	DEZ/TMA ratio	Al. content (%)	ρ (Ω*cm)	Carrier conc. (cm^{-3})	μ ($cm^2/V*s$)	Thickness (nm)
ZnO T4 100			$1.55x10^4$	$2.16x10^{14}$	1.86	35.00
ZnO T4 150	0	0	3.81	$3.84x10^{19}$	0.77	42.06
ZnO T4 200			$7.08x10^{-3}$	$1.21x10^{20}$	7.33	35.52
AZO 100:1	100	1.98	$6.65x10^{-3}$	$1.38x10^{20}$	7.06	43.34
AZO 50:1	50	2.42	$7.98x10^{-3}$	$2.00x10^{20}$	3.98	41.24
AZO 20:1	20	3.89	$8.44x10^{-3}$	$3.51x10^{20}$	2.18	42.99
AZO 10:1	10	7.14	$6.42x10^{-3}$	$5.55x10^{20}$	1.76	41.86
AZO 5:1	5	14.86	6.50	$2.16x10^{19}$	0.05	38.49

Note 2: It was not possible to electrically characterize the two AZO films with the highest Al content, AZO 1:1 and AZO 2:1.

Deriving from this conclusion, aluminum was introduced into the undoped ZnO deposited at 150 ºC to see if there were any considerable changes and how it would fare against undoped ZnO deposited at 200 ºC. The addition of a dopant proved to be a success, as can be seen in Figure 3.9 a-d, with the sample AZO 100:1 showing a carrier concentration of $1.38x10^{20}$ cm^{-3}, a resistivity of $6.65x10^{-3}$ Ω*cm and a Hall mobility of 7.06 $cm^2/V*s$. Film resistivity remained fairly stable up until an Al concentration of 7.14%, from where it increased tremendously, reaching a value of 6.5 Ω*cm, whereas both carrier concentration and Hall mobility were susceptible to higher variations, with the former increasing up to $5.55x10^{20}$ cm^{-3} and then decreasing over one order of magnitude, to $2.16x10^{19}$ cm^{-3}, and the latter steadily decreasing as films became progressively more doped, until it reached a fairly negligible value of $5.00x10^{-2}$ $cm^2/V*s$. The decrease in carrier concentration might be explained by the formation of native defects in the film, most likely zinc vacancies [30] induced by the introduction of Al. This can be substantiated by the previous EDS measurements where, despite zinc content always decreasing as more dopant is introduced, this decrease is much more prominent for concentrations above 7.14% (AZO 10:1), just as indicated in Figure 3.10. Thus, this decrease can be explained by the overwhelming rise in film defects as more Al is incorporated, whereas the introduction of carriers in lightly doped films superseded the effect of the fewer vacancies that might've been present.

On the other hand, it can be seen that when AZO films are produced with a precursor ratio of 5:1, not only does their carrier mobility drastically decrease, but it is also much lower than that of ZnO films deposited at 150 ºC, even though both samples have similar carrier concentrations. This can be ascribed to the fact that even further Al incorporation is no longer substituting the Zn atoms in the matrix but is indeed starting to promote the creation of an entirely new, highly-amorphous phase, just as shown in the SEM and GIXRD results, provided in Figure 3.6 and Figure 3.7, respectively. Unlike popular amorphous oxide semiconductors such as IGZO and ZTO which are able to maintain a high carrier mobility despite their amorphous character, a direct result of the overlap of their large, spherical heavy-metal cation s orbitals [38], AZO is not able to do so, since it does not possess these large s orbitals, leading to the inevitable decrease in mobility as this material becomes progressively less crystalline. As such, it is possible to conclude that the decrease in carrier mobility is attributed to progressively higher scattering between dopant impurities and the worsening of film crystallinity.

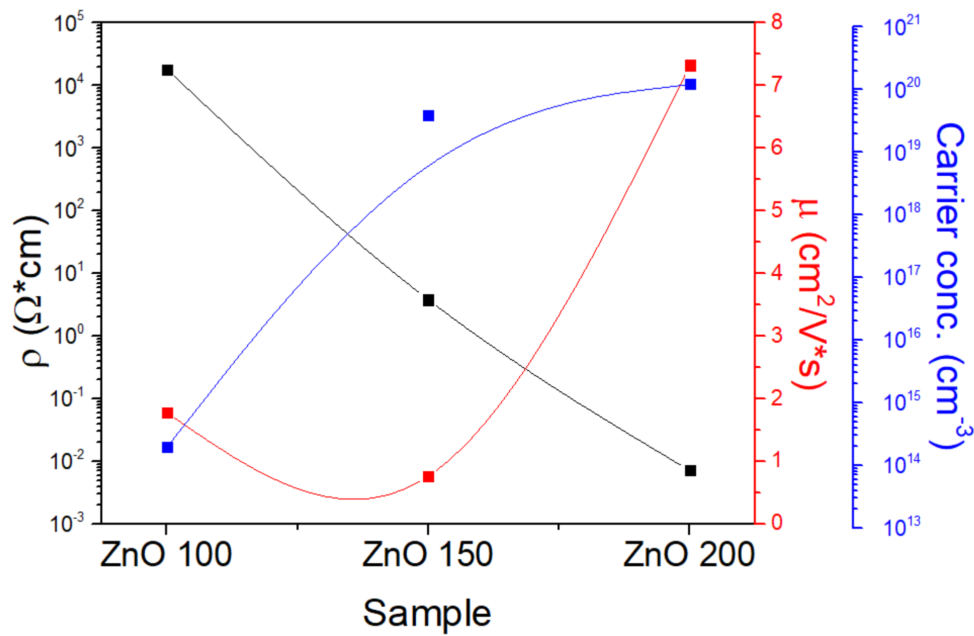

Figure 3.8. Electrical properties of ZnO films deposited using a DEZ pulse time of 0.5s in respect to substrate temperature.

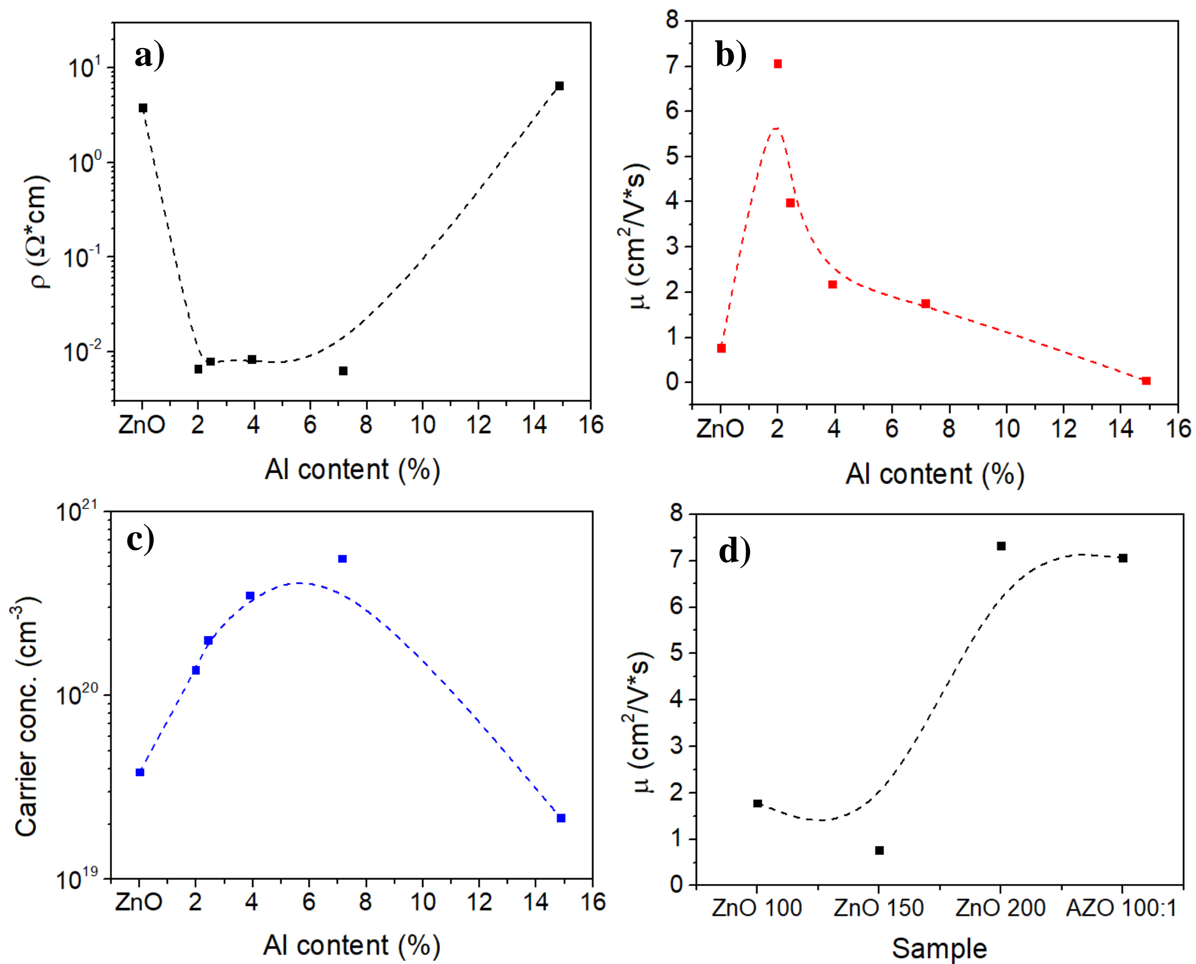

Figure 3.9. Electrical properties of AZO films for different Al concentrations. a) film resistivity, b) Hall mobility, c) Carrier concentration and d) Hall mobility of undoped vs doped ZnO.

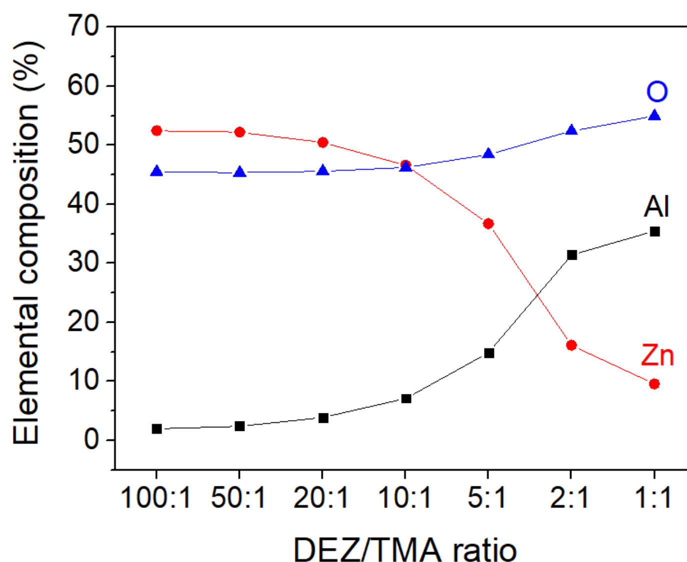

Figure 3.10. Variation in elemental composition of AZO films in regard to DEZ/TMA ratio.

3.3. XPS

3.3.1. Analysis of the ZnO/Al_2O_3 interface

In order to further study the doping mechanism, XPS measurements were performed in samples specifically deposited for this purpose, as described in Table 2, consisting of a ZnO substrate with an Al_2O_3 overlayer with varying thickness, with the full spectra for all samples being shown in Annex 6. In Figure 3.11. a) it is possible to see the high energy Zn 2p, located at approximately 1022 eV, in accordance with the binding energy value of Zn in bulk ZnO typically seen in literature, suggesting that these Zn atoms always exist in an oxidized state [39][40], with no metallic Zn being present in the films despite the thickness increase of the aluminum oxide overlayer. This can also be supported by the Zn auger emission available in Figure 3.12. where the normalized spectra shows that the peak shape, associated with ZnO [47], remains unchanged independently of overlayer thickness, further validating the notion that no metallic Zn is formed.

Figure 3.11. b) relates to the oxygen content on the AZO samples, where the XPS peak is no longer independent on the overlayer thickness. In the undoped film, the O 1s peak shows a main component centered at around 531 eV, traditionally assigned to the O^{-2} ions in the ZnO matrix, with a shoulder comprised of two smaller components located at 532 and 533 eV, attributed to oxygen vacancies and hydroxyl groups attached to Zn ions [39][41], respectively. As the effect of the overlayer becomes progressively more noticeable, an increase in the shoulder begins to occur, directly followed by a shift in the position of the peak's main component towards higher binding energies. This is possibly due to the increasing signal contributions of the O^{2-} ions in the Al_2O_3 and the oxygen associated to OH groups within the overlayer oxide [42] but, as a result of the high energy overlap between all these different peak components, the O 1s peaks were not able to be properly deconvoluted.

Finally, the Al 2p and C 1s peaks can be seen in Figure 3.11. c) and d), accordingly, with the former clearly increasing in proportion to the overlayer growth, as expected. However, a slight shift towards higher binding energies can be seen in both cases, which can be attributed to the accumulation of positive charges at the surface of the Al_2O_3, related to the photoemission process, with this phenomenon being known as differential charging. Additionally, it is possible to see that the Zn peak is not affected, suggesting that the Al_2O_3

overlayer covers the entirety of the substrate, proving that full coverage of the underlying ZnO is occurring, just like expected when using ALD.

Figure 3.11. XPS spectra of ALD-deposited ZnO films with an Al_2O_3 overlayer: a) Zn 2p peaks; b) O 1s peaks; c) Al 2p peaks; d) Zn 3s peaks

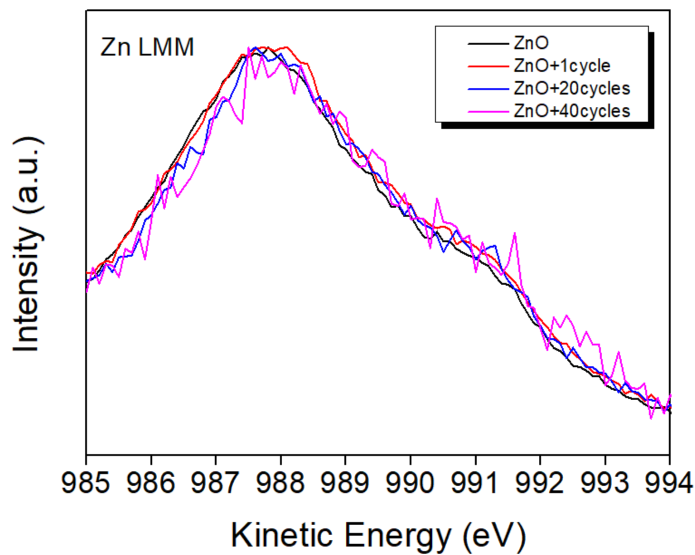

Figure 3.12. XPS spectra of the Zn Auger emission in ALD-deposited ZnO films with an Al_2O_3 overlayer

3.3.2. Overlayer thickness measurements

XPS also serves as a tool to determine film thickness, by comparing peak intensity from a substrate with that of an overlayer. The most common and popular method is presented in [43] and is stated in equation 3.1:

$$t = \lambda * cos\theta * ln\left(1 + \frac{Io/So}{Is/Ss}\right) \quad (3.1)$$

where λ corresponds to the photoelectron attenuation length in the overlayer film, determined to be approximately 2.6886, θ is the angle of emission, in this case, 0, Io and Is are the peak intensities from the overlayer and substrate respectively and finally, the So and Ss correspond to the sensitivity factors of these intensities. With this in mind, XPS was used to determine the thickness of the Al_2O_3 overlayer by using the intensities of the Zn 3s and Al 2s peaks, whose spectra can be seen in Figure 3.13. This was done in order to determine the overlayer's GPC and to see if its growth could affect the underlying substrate during the deposition. Ellipsometry measurements were also performed, with the resulting thicknesses being presented in Table 6, as to compare the results from both techniques.

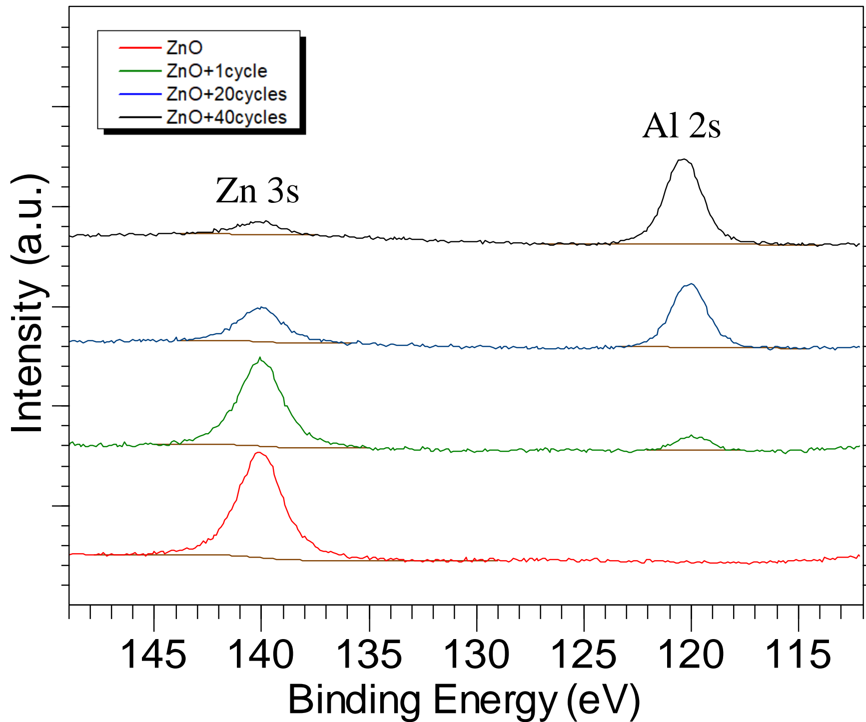

Figure 3.13. XPS spectra of Zn 3s and Al 2s obtained with the aid of CASAXPS

However, the sensitivity factors still had to be calculated. In order to do so, the approach presented by Shard et. al [44] was used. By taking into account the peak intensities of Zn 3s in the ZnO substrate and Al 2s in the Al_2O_3 overlayer, it was possible to plot the curves seen in Figure 3.14 a) and b), for the aluminum and silver X-ray sources, respectively, which were subsequently fitted with a linear model. The intersection of this fitting with the y and x axis would provide the substrate and overlayer sensitivity factors, accordingly. With this out of the way and with the aid of equation 3.1, the overlayer thickness was determined, with Figure 3.15 demonstrating the obtained results.

Table 6. Overlayer thickness of the $ZnO+Al_2O_3$ thin films determined with ellipsometry

		Overlayer thickness (nm)	Error (nm)
Sample	ZnO+1cycle	0.23	0.09
	ZnO+20cycles	1.82	0.36
	ZnO+40cycles	5.43	0.07

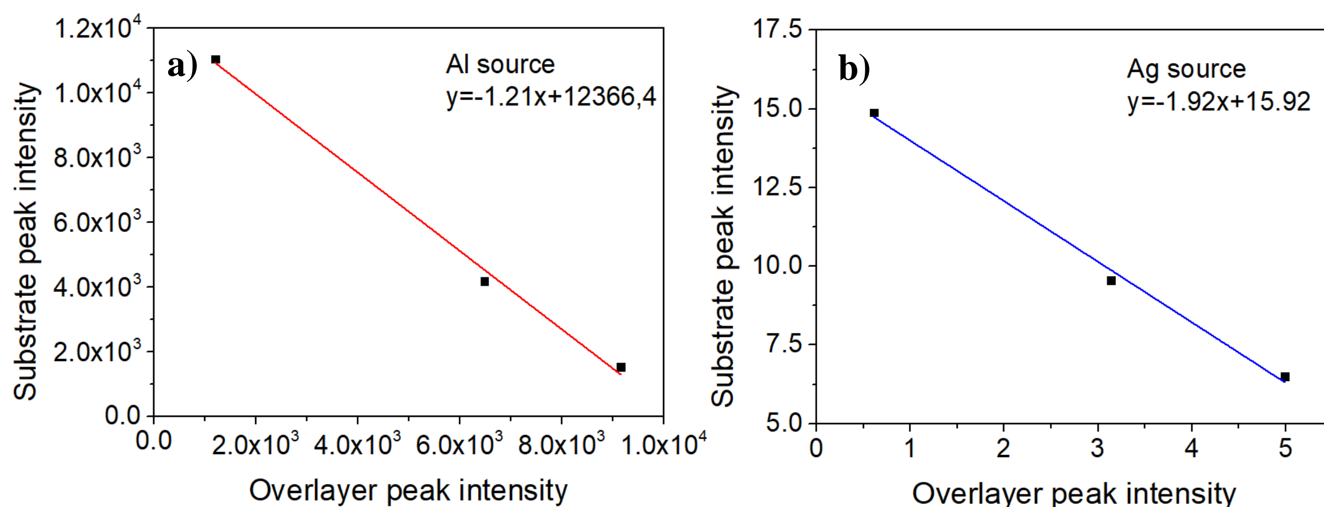

Figure 3.14. Fitting used to determine the substrate/overlayer sensitivity factors using a) an Al X-ray source and b) an Ag X-ray source

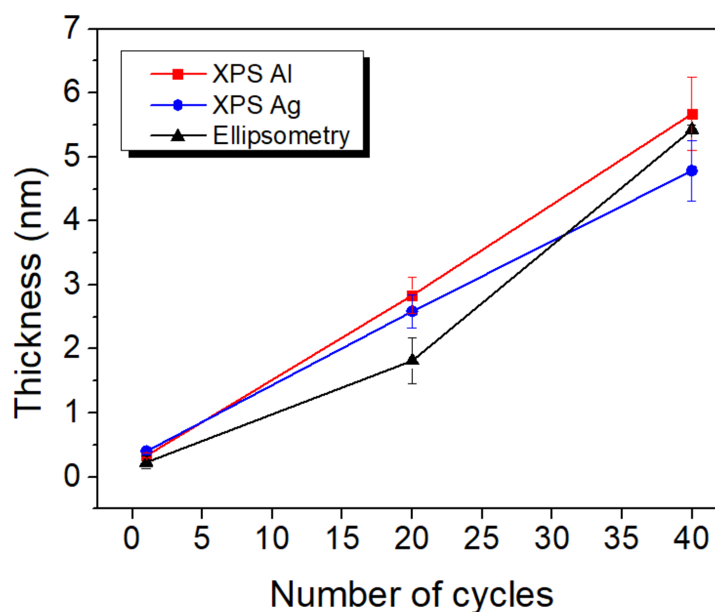

Figure 3.15. Change in Al_2O_3 overlayer thickness using different X-ray sources compared with ellipsometry data

It is possible to see in Figure 3.15. that, even though not perfect, XPS was able to provide a fairly good quantitative analysis in regard to overlayer thickness when compared to the ellipsometry data.

As explained in the Materials and Methods section, the AZO thin films that were deposited in the course of this work consisted of several ZnO cycles interspersed with individual Al_2O_3 layers and, therefore, these can be compared to the ZnO+1cycle film. Assuming that the overall ZnO thickness in both AZO and

ZnO+1cycle is the same, given the fact that the exact same deposition parameters were employed, and by averaging the thicknesses obtained for the ZnO+1cycle overlayer it is possible to determine its GPC (GPC=0.32 nm/cycle) and infer about the theoretical growth of the Al_2O_3 layers within the AZO thin films, with Table 7 presenting the expected and real AZO thickness (even though the latter was already presented in Table 5):

Table 7. Comparison between the expected and real thickness of AZO thin films

Sample	Number of Al_2O_3 layers	Avg. GPC of Al_2O_3 (nm/cycle)	Real thickness (nm)	Expected Thickness (nm)
ZnO T4 150	0	0.32	42.06	42.06
AZO 100:1	2		43.34	42.70
AZO 50:1	4		41.24	43.34
AZO 20:1	10		42.99	45.26
AZO 10:1	20		41.86	48.46
AZO 5:1	40		38.49	54.86

Note 3: For the sake of continuity, only the thicknesses of films deposited with a ratio superior to 5:1 were presented, with the data for the remaining films being shown, once again, in Annex 4, where this phenomenon is kept until a precursor ratio of 1:1, possibly due to the clash of both species and formation of a completely new phase.

Assuming that the ZnO growth remains unchanged during the deposition of doped films, it would be expected to see AZO samples steadily growing from a base thickness similar to that of undoped ZnO, as more aluminum layers are introduced. However, as can be seen, not only is the real AZO film thickness different than the one expected but, in general, as the Al content increases the real thickness of these films decreases, hinting at a possible growth inhibition of the ZnO layers that immediately precede the Al_2O_3 deposition steps. A similar behavior was observed in [45], where the deposition of an Al_2O_3 layer on top of a ZnO substrate would induce the etching of the latter and in [46], where this etching promotes the spread of aluminum atoms into the underlying ZnO layers which, ultimately, broadens the dopant distribution across the films outside the individual Al_2O_3 layers. This behavior has a severe effect on samples deposited using a lower precursor ratio where, due to the closer proximity between the "dopant layers", an overlap between the aluminum distribution might occur, inhibiting its ability to serve as a doping agent, hence the progressive deterioration of the electrical properties for highly doped films as seen in Section 3.2., and also promoting film distortion as previously observed.

As a result, not only does this etching provide a new understanding in regard to the change in electrical properties of the films, but it could also explain the general decrease in film thickness as the amount of aluminum increases, and why the GPC of the single overlayer is so high, especially compared to the average overlayer GPC in ZnO+20cycles and ZnO+40cycles (Annex 7).

4. Conclusions and Future Perspectives

The main purpose of this work was to fashion and optimize an atomic layer deposition (ALD) process of ZnO and AZO films. By employing this deposition technique, films with a very uniform and conformal surface could, in theory, be produced.

With the use of an organo-metallic precursor, DEZ, and a co-reactant, H_2O, undoped ZnO films were fabricated within a temperature window of 125-150 ºC, with a stable growth per cycle (GPC) being achieved. The growth rate and temperature window of ALD-deposited films are known to be dependent on the precursor that is utilized, with the obtained results being in full agreement with the existing literature in regard to this DEZ-based processes. As such, the rather low temperature in which ALD behavior was achieved opens the way for future film depositions on temperature-sensitive substrates, a key necessity in several technological areas such as flexible electronics. Furthermore, by introducing an additional precursor, TMA, to the already optimized ZnO process, it was possible to deposit doped ZnO films, proving that the implementation of this specific ALD super cycle was indeed feasible.

By means of infrared spectroscopy it was possible to evaluate both the efficiency of reaction byproduct elimination in the pure ZnO thin films and the effect of different dopant concentrations on the doped samples. In regard to the undoped films, the only noticeable peaks was that of the Si-O bond, attributed to the substrate that was used. The main takeaway was the evident lack of peaks associated with the C-H bond for higher wavenumbers, indicating that the purge times used were adequate and able to remove all ALD byproducts, halting their incorporation onto the films. Additionally, FTIR analysis also provided information in regard to dopant incorporation, with the appearance of a broad peak assigned to the vibrational modes of Al-O, especially in the two AZO films deposited using lower DEZ/TMA ratios, pointing out the increasing substitution of Zn atoms in the matrix by the impurities, with SEM imaging, alongside EDS analysis, corroborating this notion, since the decrease in precursor ratio is accompanied by an increase in Al content to a point where the dopant managed to “overwhelm” the zinc matrix, leading to the formation of a completely new and amorphous structure.

In order to support the findings related to the morphological structure observed with SEM, both GIXRD and XRD measurements were performed, doubtlessly proving that films with very high Al content were indeed amorphous, whereas the films fabricated with lower doping concentrations retained the polycrystalline character typically seen in ZnO.

The electrical properties of both the undoped and doped samples were characterized, in order to assess the effect of substrate temperature and dopant concentration. Concerning the case of the ZnO films, it was possible to see that films deposited at higher temperatures, 200 ºC to be precise, presented the highest carrier mobility, 7.33 $cm^2/V*s$, and the lowest film resistivity, $7.08x10^{-3}$ $\Omega*cm$, out of all the three substrate temperatures that were tested, possibly due to improved film quality. On the other hand, AZO films deposited at 150 ºC using a DEZ/TMA ratio of 100:1, therefore containing the least amount of dopant, showed a similar mobility, 7.06 $cm^2/V*s$, and a slightly lower film resistivity, $6.65x10^{-3}$ $\Omega*cm$, with progressively higher Al concentrations negatively affecting carrier mobility, even though the samples resistivity remained relatively unchanged up until ratios of 5:1. The outcome of this analysis provides a very promising prospect, that of producing ALD films using a lower thermal budget while still retaining electrical properties akin to samples deposited at higher temperatures. This, once again, paves the way for the deposition of very uniform thin films and the fabrication of electronic devices on top of flexible, temperature-sensitive substrates.

Last but not least, the interface between ZnO and Al_2O_3 was analyzed through XPS, revealing that no metallic zinc atoms exist in the films, only oxidized Zn associated with ZnO. Additionally, it was possible to verify differential charging due to a shift in the binding energies of the overlayer peaks, whereas the peaks

associated to the substrate remained unchanged, indicating that the overlayer fully coats the substrate and no island-like growth occurs. Furthermore, this technique was also able to semi-accurately determine the thickness of the Al_2O_3 overlayer when compared to ellipsometry while also hinting at the existence of Al_2O_3 promoted etching of the ZnO, hence the decrease in AZO film thickness as they become progressively more Al rich.

Hopefully this work may serve as the steppingstone when it comes to the use of ALD in the production of conducting oxides, however, some additional tests and future analysis could also be undertaken, namely the use of longer precursor pulses and subsequent comparison with lower injection times, as was intended during the development of this dissertation, and the further adjustment of the pulse/purge times of the Al_2O_3 process. Furthermore, as is expected when characterizing TCOs, the analysis of the optical transmittance and refractive index of these films could be of paramount importance, in order to assess the film quality and transparency, leading to the possible implementation in display and/or photovoltaic technologies. Last but not least, the use of post-deposition annealing processes and the incorporation of hydrogen in the films could be performed as to further improve the electrical response of these films and reduce the existing oxygen vacancies/remove the positive charges accumulated in the films as observed with the aid of XPS. Obviously, this could clash with the very notion of implementing AZO films as TCOs in temperature-sensitive devices, however, the possible improvements upon the already competent electrical response could further solidify the ALD technique as a key tool for device fabrication at CENIMAT|i3N and CEMOP.

5. REFERENCES

[1] T. Sannicolo, M. Lagrange, A. Cabos, C. Celle, J. P. Simonato, and D. Bellet, "Metallic Nanowire-Based Transparent Electrodes for Next Generation Flexible Devices: a Review," *Small*, vol. 12, no. 44, pp. 6052–6075, 2016.

[2] K. Ellmer, "Past achievements and future challenges in the development of optically transparent electrodes," *Nat. Photonics*, vol. 6, no. 12, pp. 809–817, 2012.

[3] R. W. Johnson, A. Hultqvist, and S. F. Bent, "A brief review of atomic layer deposition : from fundamentals to applications," *Biochem. Pharmacol.*, vol. 00, no. 00, pp. 1–11, 2014.

[4] D.-J. Lee, J.-Y. Kwon, S.-H. Kim, H.-M. Kim, and K.-B. Kim, "Effect of Al Distribution on Carrier Generation of Atomic Layer Deposited Al-Doped ZnO Films," *J. Electrochem. Soc.*, vol. 158, no. 5, p. D277, 2011.

[5] D. Dimitrov *et al.*, "Atomic layer-deposited al-doped ZnO thin films for display applications," *Coatings*, vol. 10, no. 6, pp. 1–12, 2020.

[6] S. Sinha, S. K. Maurya, R. Balasubramaniam, and S. K. Sarkar, "Development of Al doped ZnO as TCO by Atomic Layer Deposition," *2015 IEEE 42nd Photovolt. Spec. Conf. PVSC 2015*, pp. 6–9, 2015.

[7] B. O'Neill, "Indium market forces, a commercial perspective," *Conf. Rec. IEEE Photovolt. Spec. Conf.*, pp. 556–559, 2010.

[8] D. Lison *et al.*, "Sintered Indium-Tin-Oxide (ITO) particles: A new pneumotoxic entity," *Toxicol. Sci.*, vol. 108, no. 2, pp. 472–481, 2009.

[9] K. Nagano *et al.*, "Inhalation carcinogenicity and chronic toxicity of indium-tin oxide in rats and mice," *J. Occup. Health*, vol. 53, no. 3, pp. 175–187, 2011.

[10] С. Космического, А. Ка, П. Центра, У. Полетами, and Ф. Page, "Программы Центра Управления Полетами, Космический аппарат «Фото... Page 1 of 3," no. 800, pp. 1–3, 2008.

[11] Z. Kan, Z. Wang, Y. Firdaus, M. Babics, H. N. Alshareef, and P. M. Beaujuge, "Atomic-layer-deposited AZO outperforms ITO in high-efficiency polymer solar cells," *J. Mater. Chem. A*, vol. 6, no. 22, pp. 10176–10183, 2018.

[12] Polinares EU Policy on Natural Resources, "Fact Sheet: Indium," *Polinares Consort. 2012*, pp. 1–15, 2012.

[13] M. Lokanc, R. Eggert, and M. Redlinger, "The Availability of Indium: The Present, Medium Term, and Long Term," *Natl. Renew. Energy Lab.*, vol. October, no. October, pp. 1–90, 2015.

[14] T. Stapi, B. Swatowska, W. Powro, H. Czternastek, and G. Lewi, "Application Properties of ZnO and AZO Thin Films Obtained by the ALD Method," 2021.

[15] H. L. Shen, H. Zhang, L. F. Lu, F. Jiang, and C. Yang, "Preparation and properties of AZO thin films on different substrates," *Prog. Nat. Sci. Mater. Int.*, vol. 20, no. 1, pp. 44–48, 2010.

[16] B. Ayachi, T. Aviles, J. P. Vilcot, and C. Sion, "Rapid thermal annealing effect on the spatial resistivity distribution of AZO thin films deposited by pulsed-direct-current sputtering for solar cells applications," *Appl. Surf. Sci.*, vol. 366, pp. 53–58, 2016.

[17] H. Agura, A. Suzuki, T. Matsushita, T. Aoki, and M. Okuda, "Low resistivity transparent conducting Al-doped ZnO films prepared by pulsed laser deposition," *Thin Solid Films*, vol. 445, no. 2, pp. 263–267, 2003.

[18] S. M. George, A. W. Ott, and J. W. Klaus, "Surface {Chemistry} for {Atomic} {Layer} {Growth}," *J. Phys. Chem.*, vol. 100, no. 31, pp. 13121–13131, 1996.

[19] J. Nishizawa, T. Kurabayashi, H. Abe, and A. Nozoe, "Mechanism of surface reaction in GaAs layer growth," *Surf. Sci.*, vol. 185, no. 1–2, pp. 249–268, 1987.

[20] S. M. George, "Atomic layer deposition: An overview," *Chem. Rev.*, vol. 110, no. 1, pp. 111–131, 2010.

[21] J. Niinisto, "Atomic Layer Deposition," vol. 4, pp. 101–123, 2014.

[22] J. V. Sci, "Status and prospects of plasma-assisted atomic layer deposition," vol. 030902, no. February, 2019.

[23] R. Lo Nigro, E. Schilirò, G. Mannino, and S. Di Franco, "Comparison between thermal and plasma enhanced atomic layer deposition processes for the growth of HfO 2 dielectric layers," *J. Cryst. Growth*, vol. 539, no. March, p. 125624, 2020.

[24] de Raadt, "Spatial ALD of zinc tin oxide," *Eindhoven Univ. Technol.*, 2015.

[25] A. J. M. Mackus, J. R. Schneider, C. Macisaac, J. G. Baker, and S. F. Bent, "Synthesis of Doped, Ternary, and Quaternary Materials by Atomic Layer Deposition: A Review," *Chem. Mater.*, vol. 31,

no. 4, pp. 1142–1183, 2019.
[26] H. C. M. Knoops, S. E. Potts, A. A. Bol, and W. M. M. Kessels, "Atomic Layer Deposition," *Handb. Cryst. Growth Thin Film. Ep. Second Ed.*, vol. 3, pp. 1101–1134, 2015.
[27] J. T. Tanskanen, C. Ha, and S. F. Bent, "Correlating Growth Characteristics in Atomic Layer Deposition with Precursor Molecular Structure: The Case of Zinc Tin Oxide," 2014.
[28] M. Yu, A. Wang, Y. Wang, C. Li, and G. Shi, "An alumina stabilized ZnO-graphene anode for lithium ion batteries via atomic layer deposition," *Nanoscale*, vol. 6, no. 19, pp. 11419–11424, 2014.
[29] M. I. Hossain *et al.*, "Atomic layer deposition of metal oxides for efficient perovskite single-junction and perovskite/silicon tandem solar cells," *RSC Adv.*, vol. 10, no. 25, pp. 14856–14866, 2020.
[30] G. Luka *et al.*, "Aluminum-doped zinc oxide films grown by atomic layer deposition for transparent electrode applications," *J. Mater. Sci. Mater. Electron.*, vol. 22, no. 12, pp. 1810–1815, 2011.
[31] E. Guziewicz *et al.*, "ALD grown zinc oxide with controllable electrical properties," *Semicond. Sci. Technol.*, vol. 27, no. 7, 2012.
[32] S. I. Boyadjiev, V. Georgieva, R. Yordanov, Z. Raicheva, and I. M. Szilágyi, "Preparation and characterization of ALD deposited ZnO thin films studied for gas sensors," *Appl. Surf. Sci.*, vol. 387, pp. 1230–1235, 2016.
[33] A. J. M. Mackus, C. Macisaac, W. H. Kim, and S. F. Bent, "Incomplete elimination of precursor ligands during atomic layer deposition of zinc-oxide, tin-oxide, and zinc-tin-oxide," *J. Chem. Phys.*, vol. 146, no. 5, 2017.
[34] D. Esken *et al.*, "ZnO@ZIF-8: Stabilization of quantum confined ZnO nanoparticles by a zinc methylimidazolate framework and their surface structural characterization probed by CO2 adsorption," *J. Mater. Chem.*, vol. 21, no. 16, pp. 5907–5915, 2011.
[35] M. M. Frank, Y. J. Chabal, and G. D. Wilk, "Nucleation and interface formation mechanisms in atomic layer deposition of gate oxides," *Appl. Phys. Lett.*, vol. 82, no. 26, pp. 4758–4760, 2003.
[36] W. Choi, "Zinc oxide by ALD for thin-film-transistor application," no. Cvce 2008, pp. 751–755, 2009.
[37] "ALD of ZnO transparent conducting oxides (1997).PDF." .
[38] H. Q. Chiang, J. F. Wager, R. L. Hoffman, J. Jeong, and D. A. Keszler, "High mobility transparent thin-film transistors with amorphous zinc tin oxide channel layer High mobility transparent thin-film transistors with amorphous zinc tin oxide channel layer," vol. 013503, 2005.
[39] C. H. Zhai *et al.*, "Effects of Al Doping on the Properties of ZnO Thin Films Deposited by Atomic Layer Deposition," *Nanoscale Res. Lett.*, vol. 11, no. 1, 2016.
[40] B. R. Strohmeier and D. M. Hercules, "Surface spectroscopic characterization of the interaction between zinc ions and γ-alumina," *J. Catal.*, vol. 86, no. 2, pp. 266–279, 1984.
[41] J. H. Park, F. H. Alshammari, Z. Wang, and H. N. Alshareef, "Interface Engineering for Precise Threshold Voltage Control in Multilayer-Channel Thin Film Transistors," *Adv. Mater. Interfaces*, vol. 3, no. 24, pp. 1–7, 2016.
[42] P. K. Nayak, J. A. Caraveo-Frescas, Z. Wang, M. N. Hedhili, Q. X. Wang, and H. N. Alshareef, "Thin film complementary metal oxide semiconductor (CMOS) device using a single-step deposition of the channel layer," *Sci. Rep.*, vol. 4, pp. 1–7, 2014.
[43] P. J. Cumpson and P. C. Zalm, "Thickogram: A method for easy film thickness measurement in XPS," *Surf. Interface Anal.*, vol. 29, no. 6, pp. 403–406, 2000.
[44] A. G. Shard, "Practical guides for x-ray photoelectron spectroscopy: Quantitative XPS," *J. Vac. Sci. Technol. A*, vol. 38, no. 4, p. 041201, 2020.
[45] D. R. Zywotko and S. M. George, "Thermal Atomic Layer Etching of ZnO by a 'Conversion-Etch' Mechanism Using Sequential Exposures of Hydrogen Fluoride and Trimethylaluminum," *Chem. Mater.*, vol. 29, no. 3, pp. 1183–1191, 2017.
[46] Y. Wu *et al.*, "Dopant Distribution in Atomic Layer Deposited ZnO:Al Films Visualized by Transmission Electron Microscopy and Atom Probe Tomography," *Chem. Mater.*, vol. 30, no. 4, pp. 1209–1217, 2018.
[47] J. W. Maina *et al.*, "Atomic layer deposition of transition metal films and nanostructures for electronic and catalytic applications," *Crit. Rev. Solid State Mater. Sci.*, vol. 0, no. 0, pp. 1–22, 2020.

7. ANNEXES

Annex 1-ZnO ALD recipe

```
*Recipe ZnO
*test save
*Recipe for ZnO
*Precursors DEZ and Water by own vapor pressures
*Mim , 2008 1 July
*Based on flow chart N503256
*DEZ at liquid source 3
*Water at liquid source 4
*Source needle valves (NV-PL4 open 1 turn, NV-PL1 open 1 turn)
*reactor temperature 150

*Program start
SPROG

*Close Glove box valve
CLOSE DV-GB1

*Open the N2 main valve and chamber flow valve and make sure filling valve is closed
OPEN DV-SN1,DV-NV2
CLOSE DV-NV1

*Open main vacuum valve
OPEN DV-VP1

*Set flows
  FLOW MFC-NOVS=250
  FLOW MFC-NOPS=600

*Close pulse valves
CLOSE DV-PL1,DV-BL1
CLOSE DV-PL2,DV-BL2
CLOSE DV-PL3,DV-BL3
CLOSE DV-PL4,DV-BL4
CLOSE DV-PH1,DV-BH1,DV-BHA1
CLOSE DV-PH2,DV-BH2,DV-BHA2

*Close process gas valves
CLOSE DV-PN1
CLOSE DV-PG1
CLOSE DV-PG7,DV-PG8
```

```
CLOSE DV-PG1C

*Check the vacuum level
  WUNTIL PT-P1<10 10s

*Set temperatures
  TEMP TE-R1S=150

*wait until temperature is ok
  WUNTIL TE-R1>TE-R1S 5h

*Are temperatures ok to start the process ?
WRITE M5
WUSER YES

*open precursor hand valves
WRITE M6
WUSER YES

*Pulsing DEZ and Water 200 cycles

REPEAT 200

  Pulse DV-PL3 500ms (variable)
  Purge 8s

  Pulse DV-PL4 3s
  Purge 4s

REND


*Set temperatures
  TEMP TE-R1S=150

*Close pulse valves
CLOSE DV-PL1,DV-BL1
CLOSE DV-PL2,DV-BL2
CLOSE DV-PL3,DV-BL3
CLOSE DV-PL4,DV-BL4
CLOSE DV-PH1,DV-BH1,DV-BHA1
CLOSE DV-PH2,DV-BH2,DV-BHA2
```

*Close process gas valves
CLOSE DV-PN1
CLOSE DV-PG1
CLOSE DV-PG7,DV-PG8
CLOSE DV-PG1C

*close precursor hand valves
WRITE M7
WUSER YES

*confirm that all precursor hand valves are closed
WRITE M22
WUSER YES

*Start DEZ line purge
WRITE M39
WUSER YES

PULSE DV-PL3 2min
PULSE DV-BL3 2min

*end program
EPROG

Annex 2- Al_2O_3 ALD recipe

*Recipe Al2O3 AZO
*test save
*Recipe for Al2O3 AZO
*Precursors TMA and Water by own vapor pressures
*Mim , 2021 13 October
*Based on flow chart N503256
*TMA at liquid source 2
*Water at liquid source 4
*Source needle valves (NV-PL4 open 1 turn, NV-PL1 open 1 turn)
*reactor temperature 150

*Program start
SPROG

*Close Glove box valve

```
CLOSE DV-GB1

*Open the N2 main valve and chamber flow valve and make sure filling valve is closed
OPEN DV-SN1,DV-NV2
CLOSE DV-NV1

*Open main vacuum valve
OPEN DV-VP1

*Set flows
  FLOW MFC-NOVS=250
  FLOW MFC-NOPS=600

*Close pulse valves
CLOSE DV-PL1,DV-BL1
CLOSE DV-PL2,DV-BL2
CLOSE DV-PL3,DV-BL3
CLOSE DV-PL4,DV-BL4
CLOSE DV-PH1,DV-BH1,DV-BHA1
CLOSE DV-PH2,DV-BH2,DV-BHA2

*Close process gas valves
CLOSE DV-PN1
CLOSE DV-PG1
CLOSE DV-PG7,DV-PG8
CLOSE DV-PG1C

*Check the vacuum level
  WUNTIL PT-P1<10 10s

*Set temperatures
  TEMP TE-R1S=150

*wait until temperature is ok
  WUNTIL TE-R1>TE-R1S 5h

*Are temperatures ok to start the process ?
WRITE M5
WUSER YES

*open precursor hand valves
WRITE M6
WUSER YES
```

```
*Pulsing TMA and Water 200 cycles

REPEAT 200

  Pulse DV-PL2 150ms
  Purge 5s

  Pulse DV-PL4 500ms
  Purge 4s

REND

*Set temperatures
  TEMP TE-R1S=10

*Close pulse valves
CLOSE DV-PL1,DV-BL1
CLOSE DV-PL2,DV-BL2
CLOSE DV-PL3,DV-BL3
CLOSE DV-PL4,DV-BL4
CLOSE DV-PH1,DV-BH1,DV-BHA1
CLOSE DV-PH2,DV-BH2,DV-BHA2

*Close process gas valves
CLOSE DV-PN1
CLOSE DV-PG1
CLOSE DV-PG7,DV-PG8
CLOSE DV-PG1C

*close precursor hand valves
WRITE M7
WUSER YES

*confirm that all precursor hand valves are closed
WRITE M22
WUSER YES

*Start TMA line purge
WRITE M39
WUSER YES

PULSE DV-PL2 2min
PULSE DV-BL2 2min
```

```
*end program
EPROG
```

Annex 3-AZO ALD recipe

```
*Recipe AZO
*test save
*Recipe for AZO
*Precursors DEZ,TMA and Water by own vapor pressures
*FCT , 2021 1 Oct
*Based on flow chart N503256
*DEZ at liquid source 3
*TMA at liquid source 2
*Water at liquid source 4
*Source needle valves (NV-PL4 open 1 turn, NV-PL1 open 1 turn)
*reactor temperature 150

*Program start
SPROG

*Close Glove box valve
CLOSE DV-GB1

*Open the N2 main valve and chamber flow valve and make sure filling valve is closed
OPEN DV-SN1,DV-NV2
CLOSE DV-NV1

*Open main vacuum valve
OPEN DV-VP1

*Set flows
  FLOW MFC-NOVS=250
  FLOW MFC-NOPS=600

*Close pulse valves
CLOSE DV-PL1,DV-BL1
CLOSE DV-PL2,DV-BL2
CLOSE DV-PL3,DV-BL3
CLOSE DV-PL4,DV-BL4
CLOSE DV-PH1,DV-BH1,DV-BHA1
CLOSE DV-PH2,DV-BH2,DV-BHA2

*Close process gas valves
CLOSE DV-PN1
```

```
CLOSE DV-PG1
CLOSE DV-PG7,DV-PG8
CLOSE DV-PG1C

*Check the vacuum level
  WUNTIL PT-P1<10 10s

*Set temperatures
  TEMP TE-R1S=150

*wait until temperature is ok
  WUNTIL TE-R1>TE-R1S 5h

*Are temperatures ok to start the process ?
WRITE M5
WUSER YES

*open precursor hand valves
WRITE M6
WUSER YES

*Pulsing

REPEAT 4 (variable)

REPEAT 50 (variable)

  Pulse DV-PL3 500ms
  Purge 8s

  Pulse DV-PL4 3s
  Purge 4s
REND

  Pulse DV-PL2 150ms
  Purge 5s

  Pulse DV-PL4 500ms
  Purge 4s

REND

*Set temperatures
  TEMP TE-R1S=10
```

```
*Close pulse valves
CLOSE DV-PL1,DV-BL1
CLOSE DV-PL2,DV-BL2
CLOSE DV-PL3,DV-BL3
CLOSE DV-PL4,DV-BL4
CLOSE DV-PH1,DV-BH1,DV-BHA1
CLOSE DV-PH2,DV-BH2,DV-BHA2

*Close process gas valves
CLOSE DV-PN1
CLOSE DV-PG1
CLOSE DV-PG7,DV-PG8
CLOSE DV-PG1C

*close precursor hand valves
WRITE M7
WUSER YES

*confirm that all precursor hand valves are closed
WRITE M22
WUSER YES
*Start line purge
WRITE M39
WUSER YES

PULSE DV-BL3 2min
PULSE DV-PL3 2min
PULSE DV-BL2 2min
PULSE DV-PL2 2min

*end program
EPROG
```

Annex 4- AZO Growth with different water pulse times

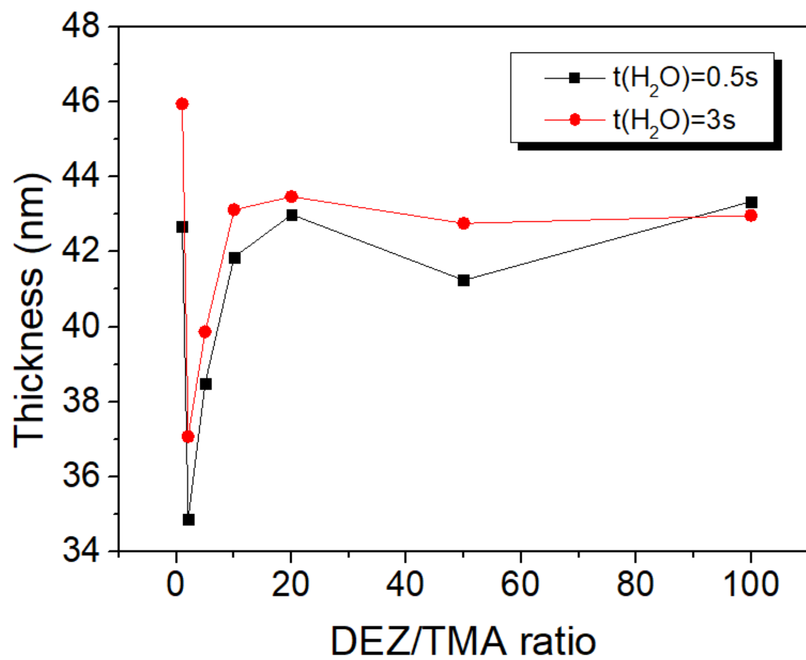

Figure A1. Thickness variation in AZO films as a function of DEZ/TMA ratio. A similar trend is observed for both water injection times

Annex 5 – XRD measurements

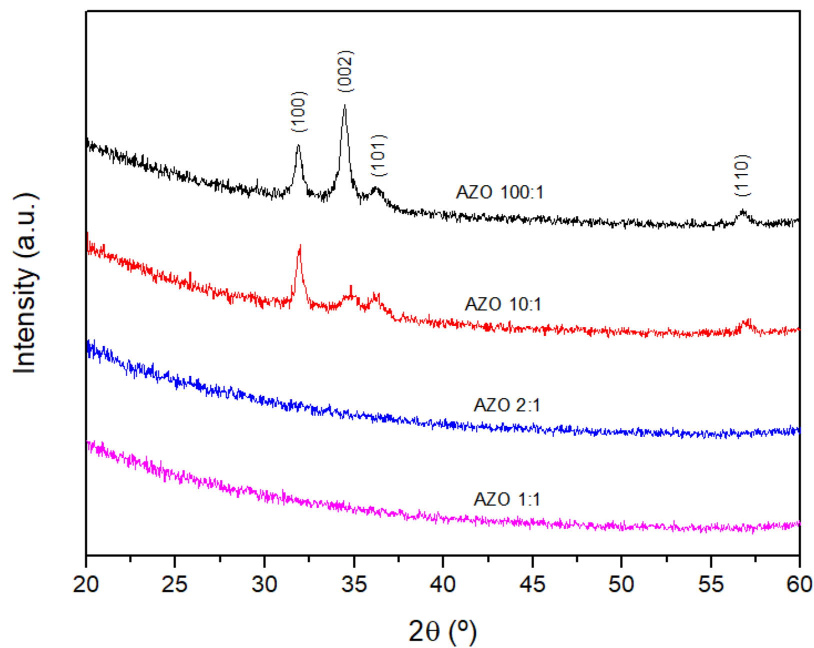

Figure A2. XRD measurements performed under a typical XRD configuration

Annex 6 – XPS full spectra

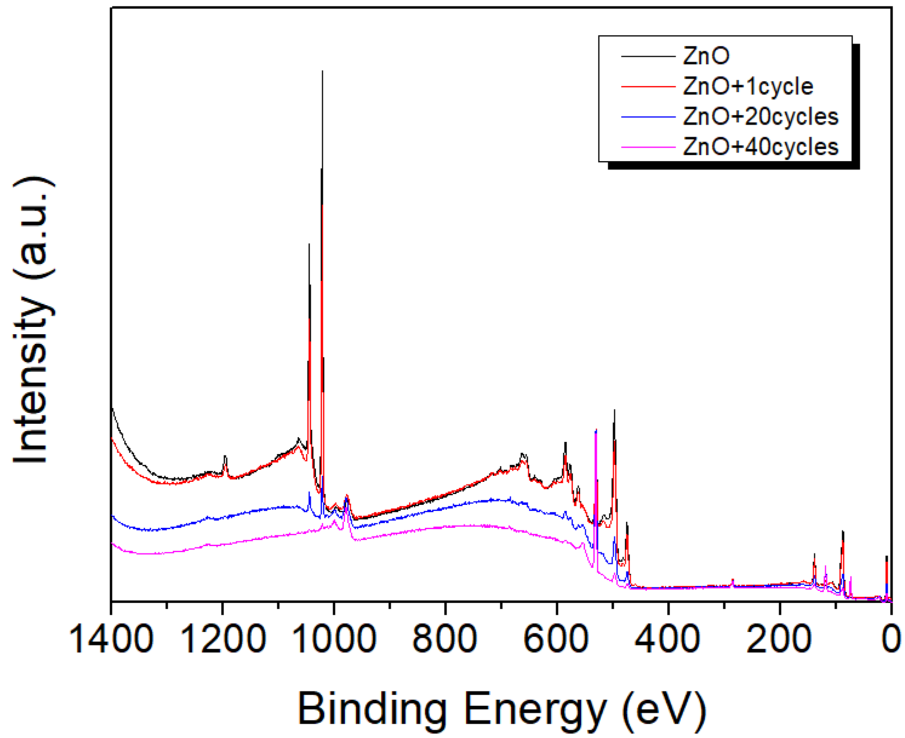

Figure A3. XPS spectra of all $ZnO+Al_2O_3$ samples deposited for this analysis.

Annex 7 – Average GPC of the Al_2O_3 overlayer

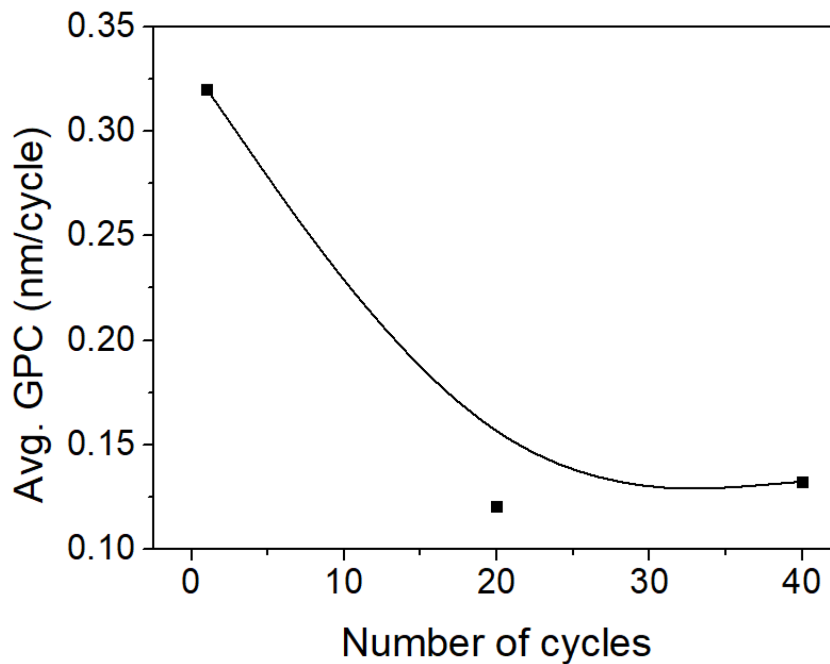

Figure A4. Variation of the overlayer GPC as the number of cycles increases.